Manuscript prepared for The Cryosphere
with version 2014/09/16 7.15 Copernicus papers of the LATEX class copernicus.cls.
Date: 7 November 2019

Glacial cycles simulation of the Antarctic Ice Sheet with PISM - Part 2: Parameter ensemble analysis

Torsten Albrecht [1], Ricarda Winkelmann [1,2], and Anders Levermann [1,2,3]

[1]Potsdam Institute for Climate Impact Research (PIK), Member of the Leibniz Association, Potsdam, Germany
[2]Institute of Physics and Astronomy, University of Potsdam, Potsdam, Germany
[3]Lamont-Doherty Earth Observatory, Columbia University, New York, USA

Correspondence to: T. Albrecht (albrecht@pik-potsdam.de)

Abstract. The Parallel Ice Sheet Model (PISM) is applied to the Antarctic Ice Sheet over the last two glacial cycles ($\approx 210,000$ years) with a resolution of 16 km. An ensemble of 256 model runs is analyzed in which four relevant model parameters have been systematically varied using full-factorial parameter sampling. Parameters and plausible parameter ranges have been identified in a companion

5   paper (Albrecht et al., 2019) and are associated with ice dynamics, climatic forcing, basal sliding and bed deformation and represent distinct classes of model uncertainties. The model is scored against both modern and geologic data, including reconstructed grounding line locations, elevation-age data, ice thickness and surface velocities as well as uplift rates. An aggregated score is computed for each ensemble member that measures the overall model-data misfit, including measurement uncertainty in

10   terms of a Gaussian error model (Briggs and Tarasov, 2013). The statistical method used to analyze the ensemble simulation results follows closely the simple averaging method described in Pollard et al. (2016).

     This analysis reveals clusters of best fit parameter combinations and hence a likely range of relevant model and boundary parameters, rather than individual best fit parameters. The ensemble of

15   reconstructed histories of Antarctic Ice Sheet volumes provides a score-weighted likely range of sea-level contributions since the Last Glacial Maximum of 9.4 ± 4.1 m (or $6.5 \pm 2.0 \times 10^6$ km^3), which is at the upper range of most previous studies. The last deglaciation occurs in all ensemble simulations after around 12,000 years before present, and hence after the Meltwater Pulse-1A. Our ensemble analysis also provides an estimate of parametric uncertainty bounds for the present-day

20   state that can be used for PISM projections of future sea-level contributions from the Antarctic Ice Sheet.

1 Introduction

Sea-level estimates involve high uncertainty in particular with regard to the potential instability of marine-based parts of the Antarctic Ice Sheet (e.g., Weertman, 1974; Mercer, 1978; Slangen et al.,
25 2017). Processed-based models provide the tools to evaluate the currently observed ice sheet changes (Shepherd et al., 2018a, b), to better distinguish between natural drift, variability or anthropogenic drivers (Jenkins et al., 2018) and to estimate future changes for possible climatic boundary conditions (Oppenheimer and Alley, 2016; Shepherd and Nowicki, 2017; Pattyn, 2018). Regarding the involved variety of uncertain parameters and boundary conditions, confidence of future projections
30 from such models is strengthened by systematic validation against modern observations and past reconstructions. We can build on experience gained in several preceding Antarctic modeling studies (Briggs et al., 2013, 2014; Whitehouse et al., 2012a; Golledge et al., 2014; Maris et al., 2014, 2015; Pollard et al., 2016, 2017; Quiquet et al., 2018), providing paleo dataset compilations or advanced scoring schemes. Modern datasets encompass ice thickness, grounding line and calving front posi-
35 tion (Bedmap2, Fretwell et al., 2013), surface velocity (Rignot et al., 2011) as well as uplift rates from GPS measurements (Whitehouse et al., 2012b). Reconstructions of grounding line location at the Last Glacial Maximum (LGM) as provided by the RAISED Consortium (Bentley et al., 2014) are used as paleo constraints as well as grounding line locations and cosmogenic elevation–age data from the AntICEdat database (Briggs and Tarasov, 2013) at specific sites during the deglaciation
40 period.

In this study we run simulations of the entire Antarctic Ice Sheet with the Parallel Ice Sheet Model (PISM, Winkelmann et al., 2011; The PISM authors, 2017). The hybrid of two shallow approximations of the stress balance and the comparably coarse resolution of 16 km allow for running
45 an ensemble of simulations of ice sheet dynamics over the last two (dominant) glacial cycles, each lasting for about 100,000 years (or 100 kyr). The three-dimensional evolution of the enthalpy within the ice sheet accounts for the formation of temperate ice (Aschwanden and Blatter, 2009; Aschwanden et al., 2012) and for the production of sub-glacial water (Bueler and van Pelt, 2015). We use the non-conserving mode of sub-glacial hydrology model, which balances basal melt rate and constant
50 drainage rate, to determine the effective pressure on the saturated till. The so-called till friction angle (accounting for small-scale till strength) and the effective pressure enter the Mohr-Coulomb yield stress criterion (Cuffey and Paterson, 2010). The yield criterion, in turn is part of the the pseudo plastic sliding law, which relates basal sliding velocity to basal shear stress.

55 PISM comes with a computationally-efficient generalization of the Elastic-plate Lithosphere with Relaxing Asthenosphere (ELRA) Earth model (Lingle and Clark, 1985; Bueler et al., 2007) with spatially varying flow in a viscous upper mantle half-space below the elastic plate, which does not require relaxation time as parameter. Geothermal heat flux based on airborne magnetic data from Mar-

tos et al. (2017), is applied to the lower boundary of a bedrock thermal layer of 2 km thickness, which

60   accounts for storage effects of the upper lithosphere and hence estimates the heat flux at the ice-bedrock interface. Climate boundary conditions are based on mean precipitation from Racmo2.3p2 (Wessem et al., 2018) and a temperature parameterization based on ERA-Interim re-analysis data (Simmons, 2006) in combination with the empirical Positive-Degree-Day method (PDD, e.g., Reeh, 1991). Climatic forcing is based on ice-core reconstructions from EPICA Dome C (EDC, Jouzel

65   et al., 2007) and WAIS Divide ice core (WDC, Cuffey et al., 2016) as well as on sea-level reconstructions from the ICE-6G GIA model (Stuhne and Peltier, 2015, 2017). Sub-shelf melting in PISM is calculated via PICO (Reese et al., 2018) from observed salinity and temperature in the lower ocean layers on the continental shelf adjacent to the ice shelves around the Antarctic continent (Schmidtko et al., 2014). Therein we consider mean values over 18 separate basins based on Zwally et al. (2015).

70   PICO updates melt rates according to changes in ocean temperatures or the geometry of the ice shelves (while changes in salinity are neglected). A description of PISM for paleo applications and sensitivity of the model to various uncertain parameter and boundary conditions are discussed in a companion paper (Albrecht et al., 2019).

75   Here, we explore uncertain model parameter ranges related to ice-internal dynamics and boundary conditions (e.g. climatic forcing, bedrock deformation and basal till properties), and use the large ensemble approach with full-factorial sampling for the statistical analysis, following Pollard et al. (2016). In view of the even larger ensemble by Briggs et al. (2014) with 31 varied parameters and over 3,000 simulations, our ensemble with only four varied parameters and 256 simulations is of

80   rather intermediate size, although we use a much finer model resolution. The analysis procedure yields an aggregated score for each ensemble simulations, which measures the misfit between PISM simulation and 9 equally weighted types of datasets. Each score can be associated with a probabilistic weight to compute the average envelope of simulated Antarctic Ice Sheet and equivalent sea-level histories and hence providing data-constrained present-day states that can be used for projections

85   with PISM.

2   Ensemble analysis

Ice sheet model simulations generally imply uncertainties in used parameterizations and applied boundary conditions. In order to generate uncertainty estimates for reconstructions of the Antarc-

90   tic Ice Sheet history and equivalent sea-level envelopes we employ an ensemble analysis approach that uses full-factorial sampling, i.e., one run for every possible combination of parameter values. We follow here closely the simple-averaging approach used in Pollard et al. (2016). This method yields as reasonable results for an adequately resolved parameter space as more advanced statistical

techniques that interpolate results between sparsely separated points in multi-dimensional parameter space. Yet, the full-factorial simple averaging method strongly limits the number of varied parameters for available computer resources, such that only the most relevant parameters for each class of climatic and boundary conditions were pre-selected (see companion paper, Albrecht et al., 2019) to cover a representative range of model responses.

2.1 Ensemble parameter

We have identified four relevant independent PISM ensemble parameters with a prior range for each parameter capturing different uncertainties in ice flow dynamics, glacial climate, basal friction and bedrock deformation. The selected parameters passed the two main criteria and (1) showed a relatively high sensitivity of the ice volume to parameter change, while (2) arriving at a present-day state with tolerable anomaly to observations, which is not at all self-evident. The four parameters and the four values used in the ensemble analysis are:

ESIA: Ice-flow enhancement parameter of the stress balance in Shallow Ice Approximation (SIA; Morland and Johnson, 1980; Winkelmann et al., 2011, Eq. 7). Ice deforms more easily in shear for increasing values of 1, 2, 4 and 7 (non-dimensional) within the Glen-Paterson-Budd-Lliboutry-Duval law. It connects strain rates $\dot{\epsilon}$ and deviatoric stresses τ for ice softness A, which depends on both liquid water fraction ω and temperature T (Aschwanden et al., 2012),

$$\dot{\epsilon}_{ij} = \text{ESIA} \cdot A(T, \omega) \, \tau^{n-1} \, \tau_{i,j} \tag{1}$$

In all ensemble runs we used for the SSA stress balance an enhancement factor of 0.6 (see Sect. 2.3 in companion paper), which is relevant for ice stream and ice shelf regions.

PPQ: Exponent q used in "pseudo plastic" sliding law which relates bed-parallel basal shear stress $\boldsymbol{\tau}_b$ to sliding velocity $\boldsymbol{u}_b$ in the form

$$\boldsymbol{\tau}_b = -\tau_c \frac{\boldsymbol{u}_b}{u_0{}^q \, |\boldsymbol{u}_b|^{1-q}}, \tag{2}$$

as calculated from the Shallow Shelf Approximation (SSA) of the stress balance (Bueler and Brown, 2009), for threshold speed u_0 and yields stress τ_c. The sliding exponent hence covers uncertainties in basal friction. Values are 0.25, 0.5, 0.75 and 1.0 (non-dimensional).

PREC: Precipitation scaling factor f_p according to temperature forcing ΔT motivated by Clausius-Clapeyron-relationship and data analysis (Frieler et al., 2015), which can be formulated as exponential function (Ritz et al., 1996; Quiquet et al., 2012) as

$$P(t) = P_0 \exp\left(f_p \, \Delta T(t)\right) \approx P_0 \left(1.0 + f_p \, \Delta T(t)\right). \tag{3}$$

For given present-day mean precipitation field P_0, the factor f_p captures uncertainty in climatic mass balance, in particular for glacial periods. Values are 2, 5, 7 and 10 %/K.

VISC: Mantle viscosity determines the characteristic response time of the linearly viscous half-space of the Earth (overlain by an elastic plate lithosphere) to changing ice and adjacent ocean loads (Bueler et al., 2007, Eq. 1). It covers uncertainties within the Earth model for values of 0.1×10^{21}, 0.5×10^{21}, 2.5×10^{21} and 10×10^{21} Pa s.

2.2 Misfit evaluation with respect to individual data-types

With four varied parameters and each parameter taking four values, the ensemble requires 256 runs. For an easier comparison to previous model studies, results are analyzed using the simple averaging method (Pollard et al., 2016). It calculates an objective aggregate score for each ensemble member that measures the misfit of the model result to a suite of selected observational modern and geologic data. The inferred misfit score is based on a generic form of an observational error model assuming a Gaussian error distribution with respect to any observation interpretation uncertainty (Briggs and Tarasov, 2013, Eq. 1).

Present-day ice sheet geometry (thickness and grounding line position) provide the strongest spatial constraint of all data-types and also offer a temporal constraint in the late Holocene. Gridded datasets are remapped to 16 km model resolution. Most of the present-day observational constraints follow closely the definitions in Pollard et al. (2016, Appendix B, Approach (A)), but weighted with each grid-cell's specific area with respect to stereographic projection. We added observed modern surface velocity as additional constraint and expanded the analysis to the entire Antarctic Ice Sheet.

1. TOTE: Mean-square error mismatch of present-day *grounded areas* to observations (Fretwell et al., 2013) assuming uncertainty in grounding line location of 30 km, as in Pollard et al. (2016, Appendix B1). Mismatch is calculated relative to the continental domain that is defined here as area with bed elevation above -2500 m.

2. TOTI: Mean-square error mismatch of present-day floating *ice shelf areas* to observations (Fretwell et al., 2013) assuming uncertainty in grounding line and calving front location of 30 km, according to Pollard et al. (2016, Appendix B2).

3. TOTDH: Mean-square-error model misfit of present-day state to observed *ice thickness* (Fretwell et al., 2013) with respect to an assumed observational uncertainty of 10 m and evaluated over the contemporary grounded region, close to Pollard et al. (2016, Appendix B3).

4. TOTGL: Mean-square-error misfit to observed *grounding line location* for the modeled Antarctic grounded mask (ice rises excluded) using a two-dimensional distance field approximation [1]. This method is different to the GL2D constraint used in Pollard et al. (2016, Appendix B5), and is only applied to the present-day grounding line around the whole Antarctic Ice Sheet according to Fretwell et al. (Bedmap2; 2013), while considering observational uncertainty of 30 km as in TOTI and TOTE above.

---

[1]https://pythonhosted.org/scikit-fmm

5. UPL: Mean-square-error model misfit to modern GPS-based uplift rates on rock outcrops at 35 individual sites using the compilation by Whitehouse et al. (2012b, Table 2) including individual observational uncertainty. Misfit is evaluated for the closest model grid point as in Pollard et al. (2016, Appendix B8), including intra-data type weighting (Briggs and Tarasov, 2013, Sect. 4.3.1).

6. TOTVEL: Mean-square error misfit in (grounded) surface ice speed compared to a remapped version of observational data by Rignot et al. (2011) including their provided grid-cell wise standard deviation, bounded below by 1.5 m/yr.

Paleo-data type constraints are partly based on the AntICEdat compilation by Briggs and Tarasov (2013, Sect. 4.2), following closely their model-data misfit computation. This compilation also includes records of regional sea-level change above present-day elevation (RSL), which has not been considered in this study, as PISM lacks a self-consistent sea-level model to account for regional self-gravitational effect of the order of up to several meters, which can be similar to the magnitude of post-glacial uplift. According to Pollard et al. (2016, Appendix B4) we evaluate past and present grounding line location along four relevant ice shelf basins.

7. TROUGH: Mean-square error misfit of modeled grounding line position along four transects through Ross, Weddell and Amery Basin and Pine Island Glacier at the Last Glacial Maximum (20 kyr BP) as compared to reconstructions by Bentley et al. (RAISED Consortium; 2014, Scenario A) and at present day compared to Fretwell et al. (Bedmap2; 2013), both remapped to model grid. An uncertainty of 30 km in the location of the grounding line is assumed as in Pollard et al. (2016, Appendix B4), but as mean over those two most confident dates and for all four mentioned troughs. In contrast to previous model calibrations, reconstructions of the grounding line position at 15, 10 and 5 kyr BP have not been taken into account here, as they would favor simulations that reveal a rather slow and progressive grounding line retreat through the Holocene in both Ross and Ronne Ice Shelf, which has not necessarily been the case (Kingslake et al., 2018).

8. ELEV: Mean of squared misfit of past (cosmogenic) surface elevation vs. age in the last 120 kyr based on model–data differences at 106 individual sites (distributed over 26 regions, weighted by inverse areal density, see Sect. 4.3.1 in Briggs and Tarasov (2013)). For each data-point the smallest misfit to observations is computed for all past ice surface elevations (sampled every 1 kyr) of the 16 km model grid interpolated to the core location and datum as part of a thinning trend (Briggs and Tarasov, 2013, Sect. 4.2). A subset of these data has been also used in Maris et al. (2015); Pollard et al. (2016, Appendix B7).

9. EXT: Mean of squared misfit of observed ice extent at 27 locations around the AIS in the last 28 kyr with dates for the onset of open marine conditions (OMC) or grounding line retreat

195   (GLR). The modeled age is computed as the most recent transition from grounded to floating ice conditions considering the sea-level anomaly. The model output every 1 kyr is interpolated down to core location and linearly interpolated to 100 yr temporal resolution, while weighting is not necessary here, as described in Briggs and Tarasov (2013, Sect. 4.2). A subset of these data has been also used in Maris et al. (2015)

2.3   Score aggregation

Each of the misfits above are first transformed into a normalized individual score for each data type i and each run j using the median over all misfits $M_{i,j}$ for the 256 simulation. The procedure closely follows Approach (A) in Pollard et al. (2016, Sect. 2.4.1). Then the individual score $S_{i,j}$ is normalized according to the median to

$$S_{i,j} = \exp\left(-M_{i,j} \,/\, \mathrm{median}(M_{i,j=1..256})\right). \tag{4}$$

As in Pollard et al. (2016) we also assume that each data type is of equal importance to the overall score, avoiding the inter-data-type weighting used by Briggs and Tarasov (2013); Briggs et al. (2014), which would favor data types of higher spatio-temporal density. Hence the aggregated score for each run j is the product of the nine data-type specific scores, according to the score definition in Approach (A) by Pollard et al. (2016)

$$S_j = \prod_{i=1..9} S_{i,j}. \tag{5}$$

This implies, that one simulation with perfect fit to eight data types, but one low individual score, yields a low aggregated score for this simulation and hence for instance a low confidence for future applications.

3   Results

3.1   Analysis of parameter ensemble

We have run the full ensemble of PISM simulation over the last glacial cycle. Figure 1 shows the aggregate scores S_j for each of the 256 ensemble members, over the 4-D space spanned by the parameters ESIA, PPQ, PREC and VISC. Each individual sub-panel shows PPQ vs. VISC, and the sub-panels are arranged left-to-right for varying PREC and bottom-to-top for varying ESIA. Scores are normalized by the best score member, which equals value 1 here.
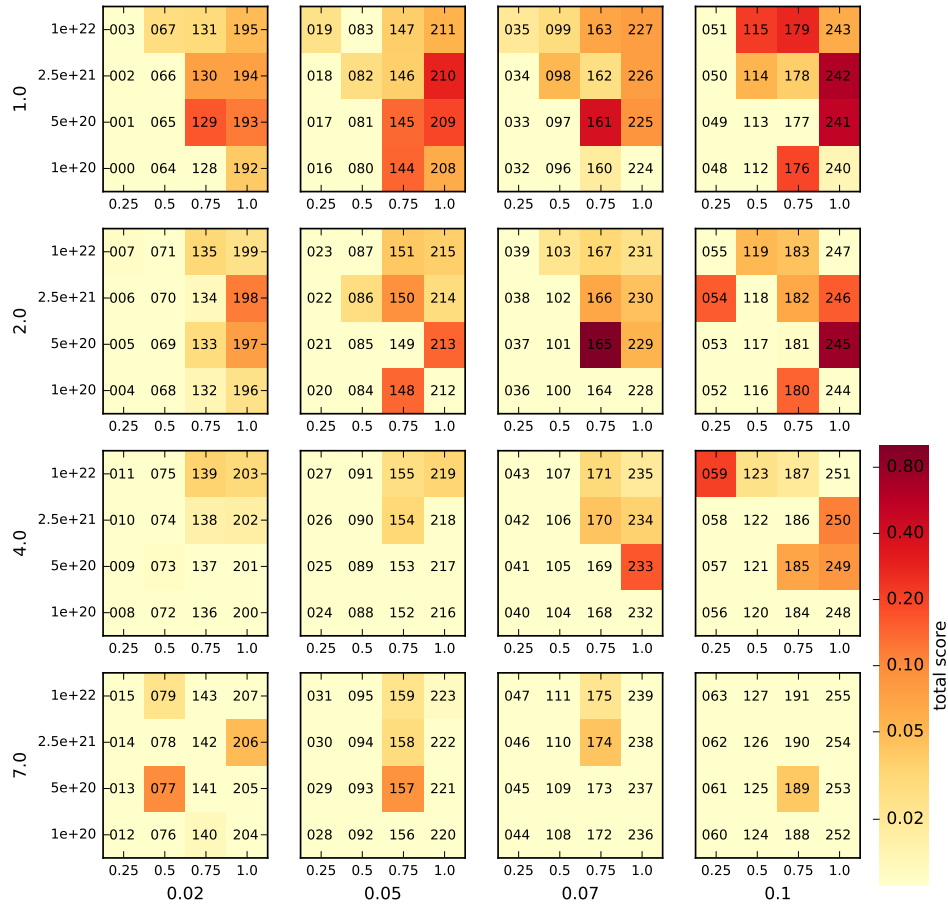
Figure 1: Aggregated score for all 256 ensemble members (4 model parameters, 4 values each) showing the distribution of the scores over the full range of plausible parameter values. The score values are computed versus geologic and modern data sets, normalized by the best score in the ensemble, and range from <0.01 (bright yellow, no skill) to 1 (dark red, best score), on a logarithmic color scale (cfs. Pollard et al., 2016, Figs. 2 + C1). The four parameters are the SIA enhancement factor ESIA (outer y-axis), the temperature-dependent precipitation scaling PREC (outer x-axis), the mantle viscosity VISC (inner y-axis) and the power-law sliding exponent PPQ (inner x-axis).

The parameter ESIA enhances the shear-dominated ice flow and hence yields ice thinning particularly in the interior of the ice sheet and therewith a decrease in the total ice volume. ESIA values of 4 or 7 have been used in other models (e.g., Maris et al., 2015) to compensate for overestimated ice thickness in the interior of East Antarctic Ice Sheet under present-day climate conditions. In our ensemble, we find a trend towards higher scores for small ESIA with values of 1 or 2 (in the upper half section of Fig. 1). This becomes more prominent when considering ensemble-mean score shares for individual parameter values as in Fig. 3, with a normalized mean score of 46% for ESIA = 1 as com-

pared to a mean score of 6% for ESIA = 7. Most of this trend is a result of the individual data-type score TOTDH (see Fig. 5, column 4, row 3) as it measures the overall misfit of modern ice thickness (and volume distribution). Partly this trend can be also attributed to the TROUGH data-type scores (Fig. 5, column 8, row 3), as for higher ESIA values grounding line motion tends to slow down, such that the time between LGM and present is not sufficient for a complete retreat back to the observed present-day location, at least in some ice shelf basins. The best-score ensemble members for small ESIA values are found in combination with both high values of mantle viscosity VISC and high values of friction exponent PPQ (center column panels in Fig. 4).

Regarding the choice of the precipitation scaling PREC the best-score members are found at the upper sampling range with values of 7 %/K or 10 %/K (see right half section in Fig. 1). Considering normalized ensemble-mean score for individual parameter values over the full range of 2–10 %/K, we can find a trend from 13% to 42% (see lowest panel in Fig. 3). Regarding combinations of parameter with PREC (left-hand column in Fig. 4), we detect a weak trend towards lower ESIA and higher PPQ, while individual data-type scores (lower row in Fig. 5) show a rather uniform pattern, in particular regarding the misfit to present-day observations. As the PREC parameter is linked to the temperature anomaly forcing, it affects the ice volume and hence the grounding line location particularly for temperature conditions different from present day. This suggests a stronger signal of PREC parameter variation in the paleo data-types scores.

A more complex pattern is found for PPQ in each of the sub-panels of Fig. 1 with highest scores for values of 0.75 and 1.0. Averaged over the ensemble and normalized over the four parameter choices we find a mean score of 5% for PPQ = 0.25 (and hence rather plastic sliding) while best scores are found for PPQ = 0.75 and PPQ = 1.0 (linear sliding) with mean scores of 40% and 46%, respectively (see second panel in Fig. 3). Best scores are found in combination with medium mantle viscosity VISC between 0.5×10^{21} Pa s and 2.5×10^{21} Pa s, as visible in the upper right panel of Fig. 4. As sliding mainly affects the ice stream flux, the trend in aggreagted score over the range of PPQ values mainly results from the velocity misfit data-type TOTVEL and grounding line position related data-types (TOTE, TOTGL and THROUGH), see Fig. 3 (second row).

Regarding mantle viscosity VISC, scores are generally low with 9% for the smallest sampled value of the parameter VISC = 0.1×10^{21} Pa s, while best scores are found in the ensemble for the five times larger viscosity of VISC = 0.5×10^{21} Pa s, with 44%. In our model, the mantle viscosity parameter has been applied to the whole Antarctic continent, although observations in some local-

ized regions as in the Amundsen Sea suggest that upper mantle viscosities could be considerably smaller than the tested range, up to the order of 10^{19} Pa s (Barletta et al., 2018). For the upper range of tested mantle viscosities, up to VISC $=10.0 \times 10^{21}$ Pa s, we find a normalized ensemble mean of 27% and 20%, respectively. Note that VISC parameter values have been sampled non-linearly over a range of two orders of magnitude. For the lowest value there is a clear trend towards smaller scores in the grounding-line and ice-thickness related data-types, such as TOTE, TOTGL, TROUGH and TOTDH respectively. As mantle viscosity determines the rate of response of the bed to changes in ice thickness a low viscosity corresponds to a rather quick uplift after grounding line retreat and hence to a retarded retreat, which corresponds to a rather extended present-day state. This implies smaller ice shelves with slower flow and less velocity misfit, such that also TOTVEL favors small VISC values. In contrast, a trend to rather high mantle viscosities in the aggregated score stems mainly from the misfit of present-day uplift rates expressed as data-type score TOTUPL, probably due to reduced sensitivity to fluctuations in grounding line location. High mantle viscosities involve a slow bed uplift and grounding line retreat can occur faster. More specifically, in the partially over-deepened ice shelf basins, which have been additionally depressed at the Last Glacial Maximum by a couple of hundred meters as compared to present, grounding line retreat can amplify itself in terms of a regional Marine Ice Sheet Instability (Mercer, 1978; Schoof, 2007; Bart et al., 2016). In fact, the best score ensemble members are found for intermediate mantle viscosities of VISC $=0.5 \times 10^{21}$ Pa s, and VISC $=2.5 \times 10^{21}$ Pa s. This could be a result of the product formulation of the aggregated score, in which individual data types scores favor opposing extreme values.

The five best-score ensemble members and associated parameter combinations are listed in Table 1. With the best-fit simulation parameters we have participated in the initMIP-Antarctica model intercomparison (Seroussi et al., 2019, PISMPAL3). The individual scores with respect to the nine data-types are visualized for the 20 best ensemble members in Fig. 2. The scores associated with the paleo data-types ELEV and EXT show only comparably little variation among the ensemble (both around 0.07 standard deviation). This also applies for the present-day ice shelf area mismatch TOTI (0.04), as no calving parameter has been varied. In contrast, present-day data types associated with velocity (TOTVEL) and uplift rates (TOTUPL) show strong variations among the 20 best ensemble members, with a standard deviation in score across the entire ensemble of 0.18 and 0.30 respectively. For data types that are related to grounding line position (TOTGL, TOTE, TROUGH) and ice volume (TOTDH) we find a similar order as for the TOTAL aggregated score (Fig. 2), with individual standard deviations in scores of 0.12-0.20 across all ensemble members. All data-type specific misfits are visualized as histogram in the Supplementary Material B (Fig. S6).

Simulation No.	ESIA	PPQ	PREC	VISC	Score	Normal. Score
165	**2.0**	**0.75**	**7 %/K**	**0.5×10^{21} Pa s**	6.1×10^{-3}	1.0
245	2.0	1.0	10 %/K	0.5×10^{21} Pa s	4.6×10^{-3}	0.76
242	1.0	1.0	10 %/K	2.5×10^{21} Pa s	3.9×10^{-3}	0.63
241	1.0	1.0	10 %/K	0.5×10^{21} Pa s	3.2×10^{-3}	0.53
261	1.0	0.75	7 %/K	0.5×10^{21} Pa s	2.4×10^{-3}	0.39

Table 1: Five best-score ensemble parameter combinations with parameter values and total scores. The best-fit simulation parameters were used in the initMIP-Antarctica model intercomparison (Seroussi et al., 2019, PISMPAL3) and for the reference simulation in the companion paper (Albrecht et al., 2019).

Comparing the ensemble-mean present-day ice thickness with observations (Bedmap2; Fretwell et al., 2013) we find regions in the inner East Antarctic Ice Sheet and in parts of the Weddell Sea sector that are about 200 m too thin, while ice thickness is overestimated by more than 500 m in the Siple Coast, in the Amery basin and along the coast line, where smaller ice shelves tend to be grounded in the simulations (Fig. 6a). Ross Sea, Weddell Sea and Amery basins show the largest ensemble-score weighted standard deviation with more than 500 m ice thickness (Fig. 6b). The ensemble spread in those basins can be associated with uncertainties in grounding line position. From its extended position at Last Glacial Maximum the grounding line has to retreat across the basins in time, with distances of up to 1000 km, leaving behind the large floating ice shelves (Fig. 7). In about 10% of the score-weighted simulations grounding line remains at the extended position without significant retreat, linked to an efficient negative feedback on grounding line motion, related to a fast responding bed (low VISC). In contrast, for rather low friction and high mantle viscosities, we find fast grounding line retreat, with a stabilization of grounding line position at or even inland of the observed location in 50% or 75% of the score-weighted simulations in the Ross and Weddell Sea sector, respectively (Fig. 8, upper panels). Due to the grounded ice retreat and the consequent unloading across the large ice shelf basins, the marine bed lifts up by up to a few hundred meters, which can lead to grounding line re-advance supported by the formation of ice rises (Kingslake et al., 2018). The ensemble mean re-advance is up to 100 km, while some of the best-score simulations reveal temporary ungrounding through the Holocene up to 400 km upstream of the present-day grounding line in the Ross sector. The Amundsen Sea sector and Amery Ice Shelf do not show such rebound effects in our model ensemble (Fig. 8, lower panels)
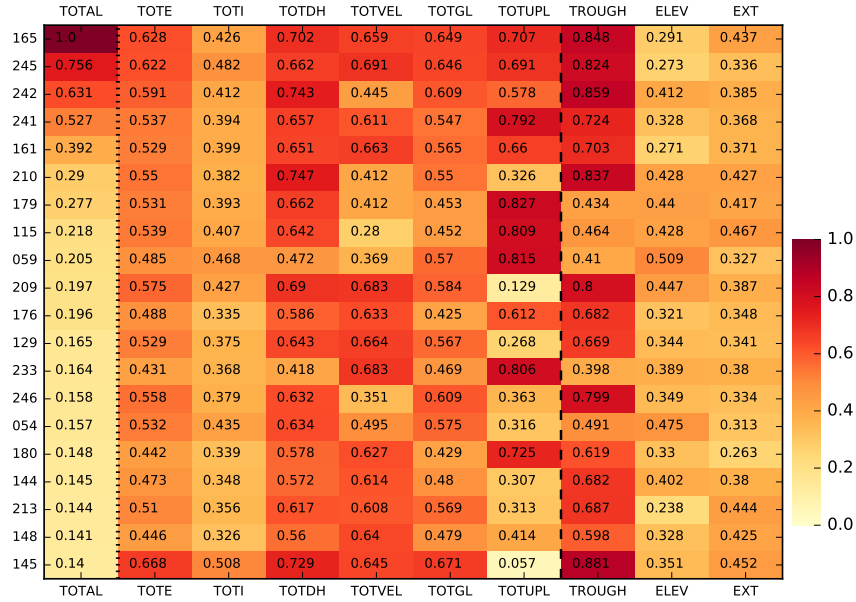
Figure 2: Aggregated and 9 individual scores for 20 best ensemble members computed versus modern and geologic data sets, divided by dashed line. The score values are normalized by the median misfit, and range from 0 (bright yellow, no skill) to 1 (dark red, best score) on a linear color scale. The standard deviation for the individual paleo data type scores ELEV and EXT, as well as for present-day ice shelf mismatch TOTI, is below 0.1. In contrast, grounding line location at LGM and present-day along four ice shelf basins (TROUGH) and present-day uplift rates (TOTUPL) have strongest impacts on the aggregated score with a standard deviation of 0.2 and 0.3, respectively. Intermediate variability of individual scores show TOTGL, TOTE, TOTDH and TOTVEL with a standard deviation between 0.1 and 0.2.
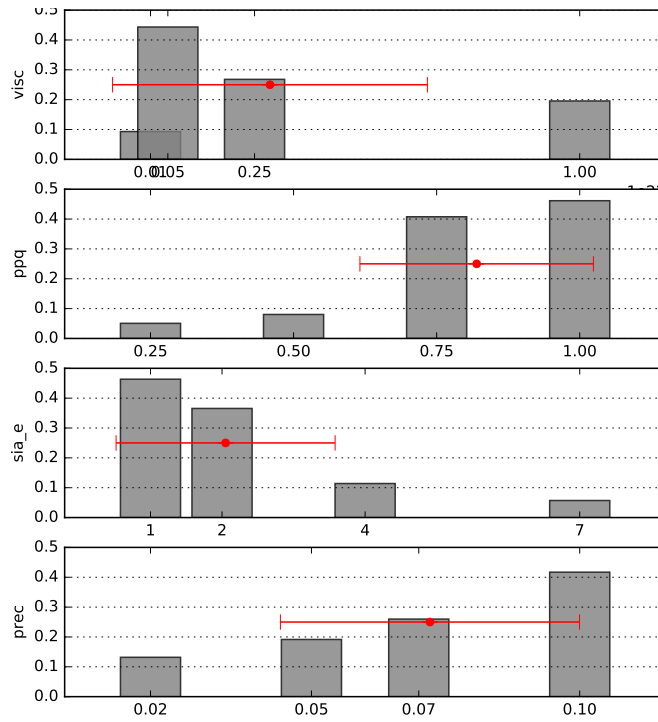
Figure 3: Ensemble-mean scores for individual parameter values (normalized such that sum is 1, or 100%). The weighted mean over the four ensemble-mean scores with standard deviation is shown in red (compare Figs. 3 + C2 in Pollard et al. (2016)).
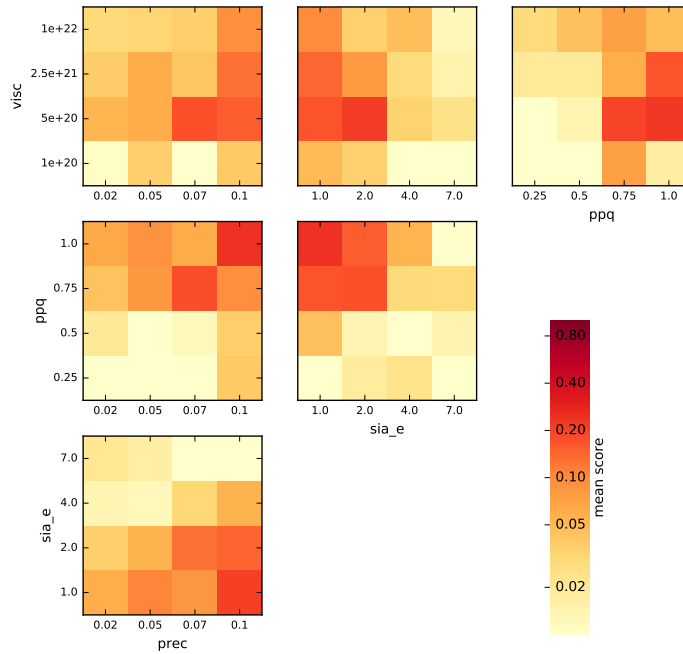
Figure 4: Ensemble-mean scores for six possible pairs of parameter values to visualize parameter dependency (compare Figs. 4 + C3 in Pollard et al. (2016)). Values are normalized such that the sum for each pair is 1. Color scale is logarithmic ranging from 0.01 (bright yellow) to 1 (red).
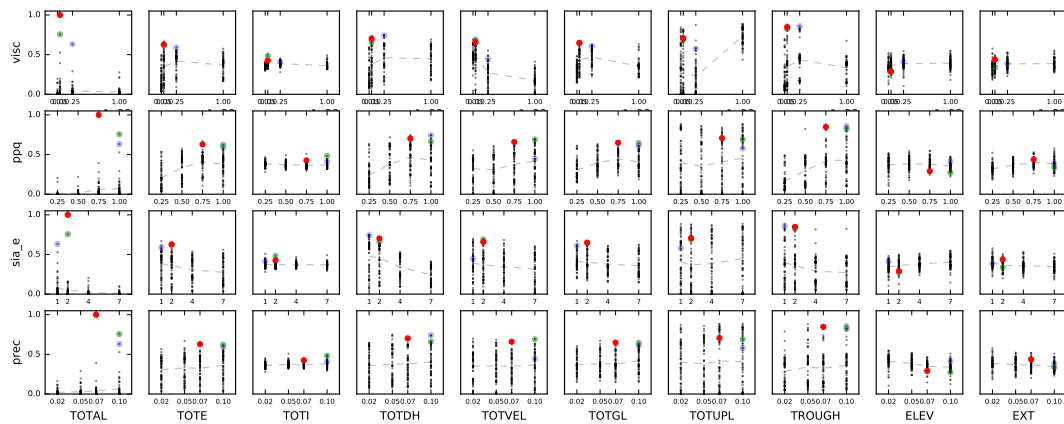
Figure 5: Scatter plot of both aggregated score and the nine individual data-type scores (panels from left to right) for each parameter setting (VISC, PPQ, ESIA and PREC as y-axis). Red dots indicate the best-score member, green and blue the second and third best ensemble members (see Table 1). Grey-dashed line indicates mean score tendency over sampled parameter range.
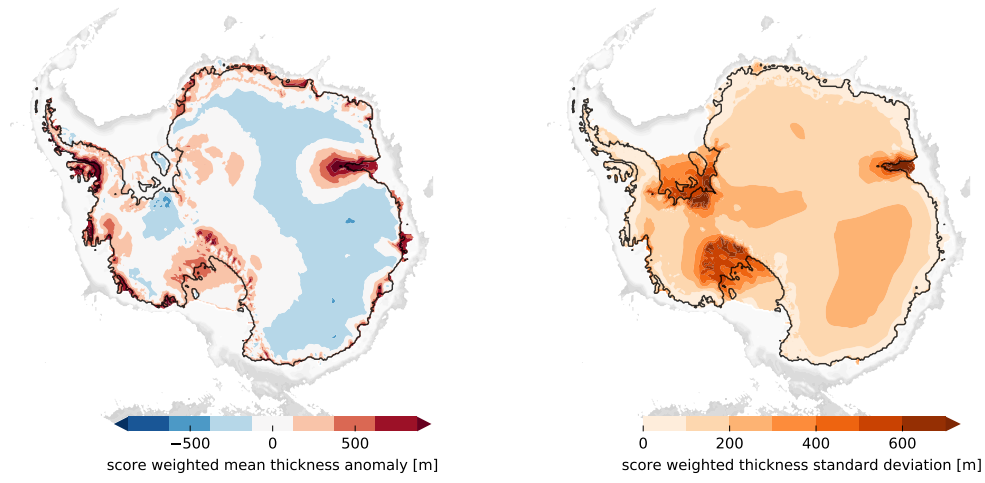
Figure 6: Score-weighted mean ice thickness anomaly to Bedmap2 (left) and score-weighted standard deviation of ice thickness (right). Ice thickness in coastal regions in West Antarctica but also in the Amery basin are generally overestimated. Amery and Filchner-Ronne Ice Shelves and Siple Coast region reveal the highest standard deviation in reconstructed present-day ice thickness among the ensemble members.
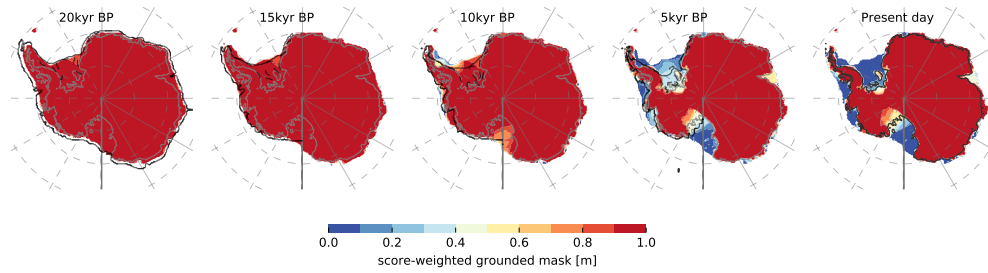
Figure 7: Ensemble-score weighted grounded mask for 5 kyr snapshots. Mask value 1 (red) indicates grounded area which is covered by all simulations, while blueish colors indicate areas which are covered only by a few simulations with low scores (compare Fig. D4 in Pollard et al. (2016)). For the last two snapshots, grounding line in the Ross Sea and Weddell Sea sector is found in about 50% of score-weighted simulations inland of its present location (Fretwell et al., 2013, grey line) with some grounding line re-advance (Kingslake et al., 2018; Siegert et al., 2019). In contrast less than 10% show no grounding line retreat from glacial maximum extent. Black lines indicate reconstructions by the RAISED Consortium (Bentley et al., 2014, Scenario B solid and scenario A dashed).
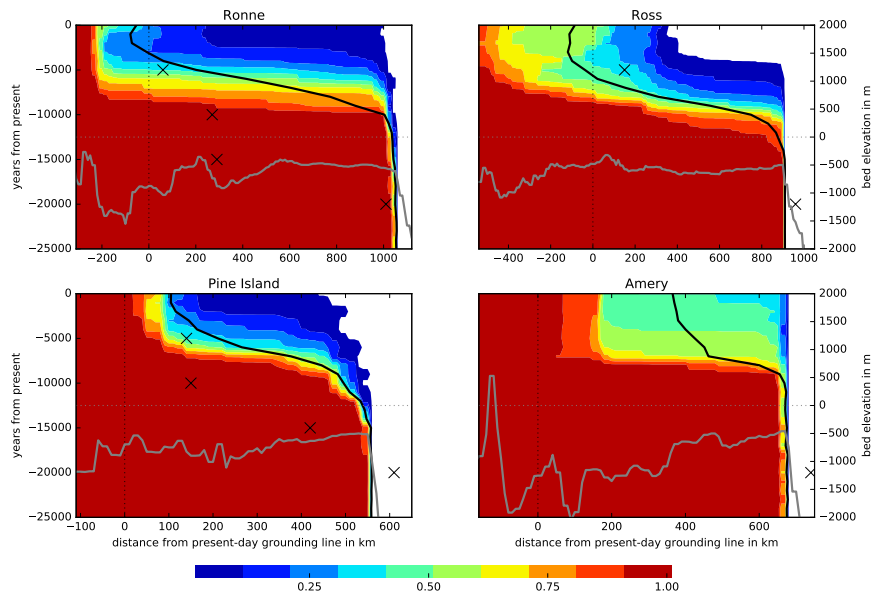
Figure 8: Ensemble score-weighted grounded ice cover along transects trough Weddell, Ross, Amundsen and Amery Ice Shelf basins over the last 25 kyr simulation period (left y-axis, compare Fig. D5 in Pollard et al. (2016)). Grounded areas which are covered by all simulations are indicated by value 1 (red), while blueish colors indicate areas which are covered only by some simulations (or those with low scores). Grounding line in the Ross Sea and Weddell Sea sector is found inland of its present location (vertically dotted) within the last 10 kyr simulation time in about 50% and 75% of score-weighted simulations, respectively. The score-weighted mean curve (black) reveals re-advance of the grounding line of up to 100 km in about 20% of the score-weighted simulations, both in the Ross and Weddell Sea sector, as discussed in (Kingslake et al., 2018). Such behavior is not found in the Pine Island trough, where grounding line retreat stops in 90% of the simulations at about 200 km downstream of its present day location. Similar in the Amery Ice Shelf, where in 30% of score-weighted simulations the ice shelf does not retreat at all from its LGM extent. Bed topography (Bedmap2; Fretwell et al., 2013) along the transect is indicated as gray line with respect to the right y-axis. For the four troughs, the data type TROUGH is evaluated for the two time slices corresponding to LGM (20 kyr BP) and present.

3.2 Reconstructed sea-level contribution histories

The full parameter ensemble is based on four simulations starting in the penultimate interglacial (210 kyr BP). These four simulations use four different values of mantle viscosity covering two orders of magnitude (VISC $= 10^{20} - 10^{22}$ Pa s). They show quite a consistent maximum ice volume at the penultimate glaciation around 130 kyr BP (see violet lines in Fig. 9). Due to the different Earth response times associated with varied mantle viscosities, the curves branch out when the ice sheet

retreats. Those four simulations were used as initial states at 125 kyr BP for the other 252 simulations of the ensemble. At the end of the Last Interglacial stage (LIG, Eemian) at around 120 kyr BP, when the full ensemble has been run for only 5 kyr, the ensemble mean ice volume is 1.0 m SLE below modern with a score-weighted standard deviation of around 2.7 m SLE (volume of grounded ice above flotation in terms of global mean sea level equivalent as defined in Albrecht et al. (2019)). This corresponds to a grounded ice volume anomaly in relation to present day observations of -$0.3 \pm 1.4 \times 10^6$ km^3. These numbers may not reveal the full possible ensemble spread as simulations still carry some memory of the previous glacial cycle simulations with different parameters. On average, grounding lines and calving fronts retreat much further inland at LIG than for present-day conditions. Yet, complete collapse of West Antarctic Ice Sheet (WAIS) does not occur in any of the ensemble members, most likely as a result of intermediate till friction angles and hence higher basal shear stress underneath the inner WAIS (see optimization in Albrecht et al. (2019)). In the case of triggered WAIS collapse one could expect an Antarctic contribution to the Eemian sea-level high stand of 3–4 m SLE (Sutter et al., 2016). Also previous paleo model studies estimate the Antarctic contribution to be at least 1 m SLE, based on a globally integrated signal, and likely significantly more, depending on Greenland's contribution (Cuffey and Marshall, 2000; Tarasov and Peltier, 2003; Kopp et al., 2009). This value has been thus used as lower bound in terms of a "sieve" criterion in previous Antarctic model ensemble analysis (Briggs et al., 2014).

Assuming, that the memory of the previous spin-up has vanished at the Last Glacial Maximum (in our simulations at around 15 kyr BP), the model ensemble yields a range of (grounded) Antarctic Ice Sheet volume of 9.4 ± 4.1 m above present-day observations, or $6.5 \pm 2.0 \times 10^6$ km^3. The histogram of score-weighted sea-level anomalies of all simulations at Last Glacial Maximum actually reveals four distinct maxima at around 4.5, 8.1, 9.0 and 13.0 m SLE (Fig. 10 a), which can be attributed to the five best-score simulations in Table 1. The ensemble spread is hence relatively wide, but still quite symmetric, as comparison with the normal distribution reveals. As expected, the LGM ice volume increases for lower PPQ (on average 3 m SLE), lower PREC (on average more than 6 m SLE) and lower ESIA values (more than 12 m SLE on average), while it seems to be rather insensitive to the choice of VISC (less than 0.5 m SLE on average). When comparing simulated volumes at Last Glacial Maximum to modeled present-day volumes (such that model biases cancel out) the model ensemble yields 10.0 ± 4.1 m of global mean sea level equivalents, or $5.8 \pm 2.0 \times 10^6$ km^3.

Most of the deglacial retreat from LGM extent and hence most of Antarctica's sea-level rise contribution occurs in our simulations after 10 kyr BP (cf. Fig. 10 b, c). In particular, for higher mantle viscosities we find episodic self-amplified retreat with change rates of more than 0.5 cm SLE per year in West Antarctic basins (in the best-fit simulation at 7.5 kyr BP, see below in Sect 3.3). This leads in some cases to grounding line retreat beyond its present location and subsequent re-advance

during Holocene, due to the uplift of the bed (discussed in Kingslake et al., 2018). However, these rapid episodes of retreat occur in our simulations consistently after Meltwater pulse 1A (MWP1a, around 14.5 kyr BP, see dashed line in Fig. 9). This delay supports the idea, that Antarctic Ice Sheet retreat has not been a source but rather a consequence of the relatively quick rise in global mean sea-level by about 15 m within 350 yr or ≈ 4 cm/yr at MWP1a (Liu et al., 2016), while core analysis of iceberg-rafted debris suggest earlier and stronger recession of the Antarctic Ice Sheet at the time of MWP1a (Weber et al., 2014). The MWP1a initiated the Antarctic Cold Reversal (ACR), a period lasting for about two millenia with colder surface temperatures. This cooling induced a freshening of surface waters and lead to a weakening of Southern Ocean overturning, resulting in reduced Antarctic Bottom Water formation, enhanced stratification and sea-ice expansion. This could have caused an increased delivery of relatively warm Circumpolar Deep Water onto the continental shelf close to the grounding line and hence to stronger sub-shelf melt (Golledge et al., 2014; Fogwill et al., 2017). As our sub-shelf melting module is forced with a modified surface temperature anomaly forcing, PICO responds with less melt during ACR period and hence prohibits significant ice sheet retreat. But even if the intermediate ocean temperature would rise by 1 or 2 K during ACR, the induced additional melt would correspond to less than -1 mm/yr SLE and hence far less than the value of -6 mm/yr SLE found by Golledge et al. (2014) (see also Albrecht et al. (2019) for the corresponding sensitivity analysis). Also MWP1b around 11.3 kyr BP occurred well before deglacial retreat initiated in most simulations of our model ensemble (see Fig. 9 c). The selection criteria for the used ensemble parameters may not sufficiently represent the onset and rate of deglaciation. One key parameter for the onset of retreat could be the minimal till friction angle on the continental shelf with values possibly below 1.0° and the availability of till water at the grounding line. More discussion of the interference of basal parameters in terms of an additional (basal) ensemble analysis is given in the Supplementary Material A.

The timing of deglaciation and possible rebound effects can explain a natural drift in certain regions that lasts through the Holocene until present-day. In the score-weighted average the ensemble simulations suggest a sea-level contributions over the last 3,000 model years of about 0.25 mm/yr, while for the reference simulation the Antarctic ice above flotation is on average even slightly growing (cf. Fig. 9 c), partly explained by net uplift in grounded areas (Fig. 12).
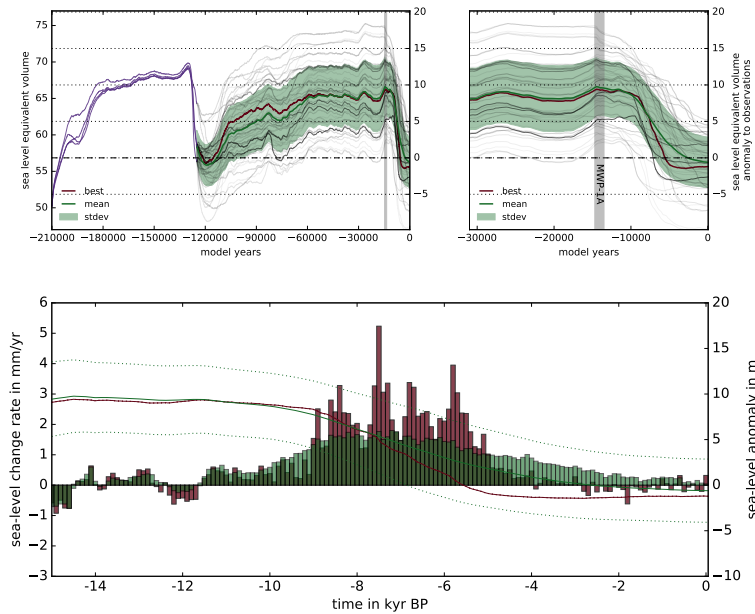
Figure 9: Simulated sea-level relevant ice volume histories over the last two glacial cycles (upper) and for last deglaciation (middle), for all 256 individual runs of the parameter ensemble, transparency-weighted by aggregated score. Red line indicates the best-score run, the green line and shading indicates the score-weighted ensemble mean and standard deviation, respectively. At Last Glacial Maximum (here at 15 kyr BP) the reconstructed ensemble-mean ice volume above flotation yields 9.4±4.1 m SLE above present-day observation (compare to Figs. 5 + C4 in Pollard et al. (2016)). Violet lines indicate simulations over the penultimate glacial cycle with four different mantle viscosities, from which the full ensemble branches at 125 kyr BP. During deglaciation the score-weighted ensemble mean (green) shows most of the sea-level change rates (lower panels) between 9 kyr BP and 5 kyr BP with mean rates above 1 mm yr^{-1}, while the best-score simulation (red) reveals rates of sea-level rise of up to 5 mm yr^{-1} (100 yr bins) in the same period (cf. Golledge et al., 2014, Fig. 3 d). In contrast to the ensemble mean, the best-score member (red line) shows a minimum ice volume in the mid-Holocene (around 4 kyr BP) and subsequent regrowth.
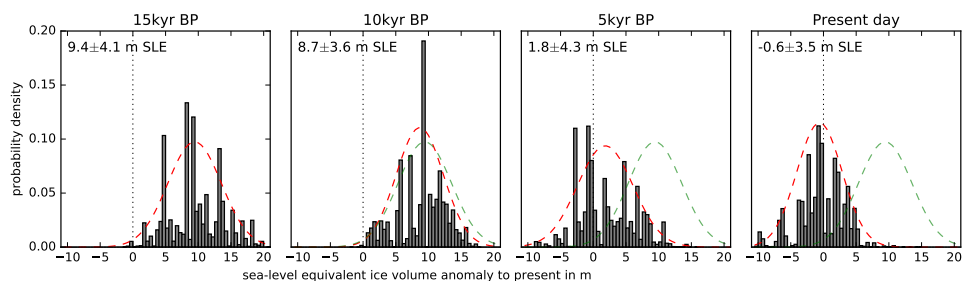
Figure 10: Equivalent global-mean sea-level contribution (ESL) relative to modern at every 5 kyr over the last deglaciation period. Grey bars show the score-weighted ensemble distribution (0.5 m bins), the red curve indicates the statistically likely range (normal distribution) of the simulated ice volumes with width of 1-sigma standard deviation as for the green envelope in Fig. 9, green gaussian curve from 15k kyr snapshot for comparison (compare to Figs. 6 + C5 in Pollard et al. (2016)).

395   The simulations are based on the Bedmap2 dataset (Fretwell et al., 2013), remapped to 16 km resolution, which corresponds to a total grounded modern Antarctic Ice Sheet volume of 56.85 m SLE (or 26.29×10^6 km^3). The ensemble mean at the end of the simulations (in the year 2000 or -0.05 kyr BP) underestimates the observed ice volume slightly by 0.6 ± 3.5 m SLE, or in terms of grounded ice volume by $0.7 \pm 1.7 \times 10^6$ km^3 (see Fig. 9). The histogram of score-weighted sea-level

400   anomalies at the end of all simulations can be well approximated by a normal distribution (Fig. 10 d). As for the LGM ice volume the ESIA parameter is responsible for most of the ice volume ensemble range at present day with more than 10 m SLE, while PREC has almost no effect with less than 1 m SLE on average, in contrast to the LGM, as expected. VISC and PPQ reveal on average a range for the present-day ice volume of about 6 m SLE and 5 m SLE, respectively.

405   **3.2.1   Comparison of LGM sea-level estimates in previous studies**

For the maximum Antarctic ice volume at the Last Glacial Maximum, the inferred ensemble range of 5.3 - 13.5 m SLE excess relative to observations (or 4.5 - 8.5 $\times 10^6$ km^3) is at the upper range found in the recent literature (Fig. 11), except for the "GRISLI" model results (Quiquet et al., 2018). The other previous model reconstructions are based on four different models: "Glimmer" (Rutt et al.,

410   2009), "PSU-ISM" (or PennState3D) from Penn State University (Pollard and DeConto, 2012a), "ANICE" from Utrecht University (De Boer et al., 2013) and, as in this study, the Parallel Ice Sheet Model (PISM; Winkelmann et al., 2011). This section briefly compares the different model and ensemble approaches with regard to the inferred LGM ice volume estimate.

415   Whitehouse et al. (2012a) ran 16 Glimmer simulations at 20 km resolution with varied sliding and isostasy parameter, and different inputs for the geothermal heat flux, climatic forcing and sea-surface height. They used both geological and glaciological data to constrain the reconstruction and

found the best fit simulation at the lower end of their ensemble ice volume range. Golledge et al. (2012) and Golledge et al. (2013) used PISM on a 5 km grid for an equilibrium simulation under LGM conditions, while Golledge et al. (2014) retrieved their ensemble mean estimates, relative to observations (Bedmap2), from an ensemble of around 250 PISM deglaciation simulations at 15 km resolution, with varied basal traction and ice-flow enhancement factors. ANICE simulations have been run on 20 km resolution. In a sensitivity study, Maris et al. (2014) varied enhancement factors, till strength and ("ELRA") bedrock deformation parameters, while in Maris et al. (2015), a small ensemble of 16 simulations with different sea-level and surface temperature forcings have been applied to two different bed topographies over the last 21 kyr. Quiquet et al. (2018) varied four parameters (SIA enhancement, friction coefficient, sub-shelf melt and subglacial hydrology) in 600 equilibrium ensemble simulations with GRISLI for 40 km resolution. They selected the 12 best thickness fit parameters to run transient simulations over the last four glacial cycles. The relatively high estinate fo LGM ice volume is likely due to the simplified basal drag computation that does not take into account bedrock physical properties (e.g. sediments). The estimates by Briggs et al. (2014) are based on (the best 178 of) a really large ensemble of more than 3,000 PSU-ISM simulations over the last two glacial cycles with 40 km resolution, coupled with a full visco-elastic isostatic adjustment bedrock response with radially layered earth viscosity profile and different treatments of sub-shelf melt, basal drag, climate forcing, and calving (in total 31 varied parameters). The full ensemble range is certainly much larger, but additional constraints allow for a selection of the most realistic simulations, with most confidence in the lower part of the given range (purple error bar in Fig. 11). Pollard et al. (2016) and Pollard et al. (2017) used the PSU-ISM on 20 km resolution for an ensemble of each 625 simulations over the last 20 kyr and varied four parameters related to sub-shelf melt, calving, basal sliding and viscous Earth deformation, while other parameters were supposedly constrained by earlier studies. Pollard et al. (2016) applied an ELRA Earth model applied to the West Antarctic Ice Sheet only, while (Pollard et al., 2017) simulated whole Antarctica coupled to a global Earth-sea level model. In both ensembles, ice volume change since LGM is somewhat biased to comparably low values, as the used scoring algorithm pushed the ensemble to rather slippery basal sliding coefficient on modern ocean beds. As Whitehouse et al. (2012a), Golledge et al. (2014) and this study provided anomalies based on the volume-above-flotation calculation (VAF), the corresponding SLE values are smaller than the directly converted values (Fig. 11b). For a conversion factor of $c = 2.5$ our study would yield 12.5 – 16.5 m SLE instead. For the LGM ice volume excess relative to the modeled present day our study yields 5.9 – 14.1 m SLE (or 3.8 - 7.8 $\times 10^6$ km^3), both indicated in Fig. 11.

3.3 Best-fit ensemble simulation

The best-fit ensemble member simulation (no. 165, see Table 1) provides an Antarctic Ice Sheet configuration for the present day, which is comparably close to observations. Yet, the present-day

(a)   (b)
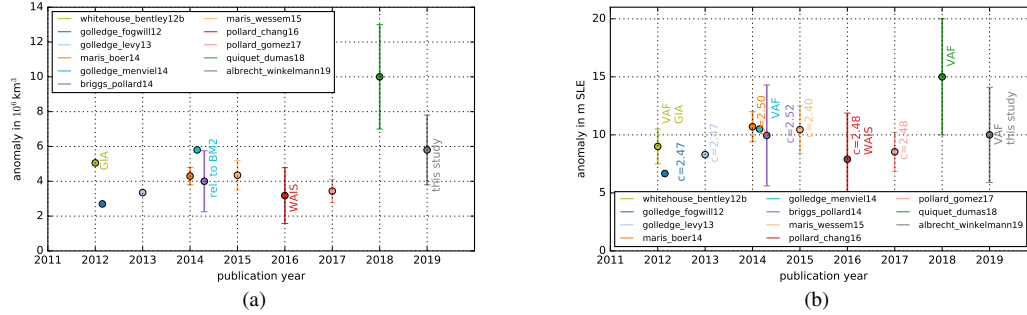
Figure 11: Ice volume anomaly between Last Glacial Maximum as compared to present (not observations) in recent modeling studies in units of 10^6 km^3 (a) and in units of meters sea-level equivalents (b). Note that the study by Pollard et al. (2016) only considers the West Antarctic subdomain in their analysis (redish). Golledge and colleagues and this study used PISM (blue and grey), Maris and colleagues used ANICE (orange), Whitehouse and colleagues used GLIMMER simulations (olive), GRISLI simulations by Quiquet and colleagues (green) and Briggs and Pollard and colleagues used PennState3D (or PSU-ISM) as model (blueish) coupled to different Earth models. Be aware, that ice volume estimates are based on different ice densities in the different models and that different conversion factors c have been used. This study, Golledge et al. (2014), as well as the Glimmer and GRISLI model provided the volume above flotation (VAF), which substracts some portion of the ice volume in panel (b). The provided uncertainty ranges are not necessarily symmetric, e.g. the upper range in Briggs et al. (2014) has less confidence than the lower range.

ice volume of the West Antarctic Ice Sheet is overestimated (by around 25%), while the much larger
455   East Antarctic Ice Sheet (EAIS) volume is rather underestimated (by around 5%), which is also
valid for the ensemble mean (Fig. 6). Part of the overestimation can be explained by the relatively
coarsely resolved topography of the Antarctic Peninsula and weakly constrained basal friction in the
Siple Coast and Transantarctic Mountain area. This results in a root-mean-square error (RMSE) of
ice thickness of 266 m (see Fig. 12 a), a RMSE of grounding line distance of 67 km (see Fig. 13)
460   and a RMSE for surface velocities of 66 m/yr (see Fig. 14). The best-fit simulation also reproduces
the general pattern of observed modern isostatic adjustment rates (see Fig. 12 b) with highest uplift
rates of more than 10 mm yr^{-1} in the Weddell and Amundsen Sea Region in agreement with GIA
model reconstructions (cf. Argus et al., 2014, Fig. 6). In contrast to these GIA reconstructions, our
best-fit simulation shows depression rather than uplift in the Siple Coast regions as grounded ice is
465   still re-advancing and hence adding load.

(a)   (b)
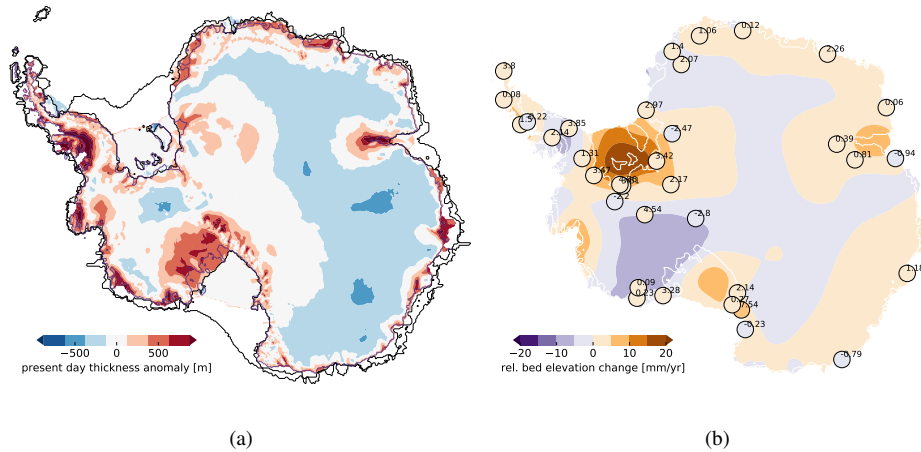
Figure 12: (a) Present-day ice thickness anomaly of best fit ensemble simulation with respect to observations (Fretwell et al., 2013), with the continental shelf in grey shades. Blue line indicates observed grounding line, while black lines indicate modeled grounding line and calving front. Large areas of the East Antarctic Ice Sheet are underestimated in ice thickness, while some marginal areas along the Antarctic Peninsula, Siple Coast and Amery Ice Shelf are thicker than observed, with a total RMSE of 266 m. (b) Modeled uplift (violet) and depression (brown) at present-day state as compared to uplift rates from recent GPS measurements (Whitehouse et al., 2012b) in 35 locations (in units mm/yr).
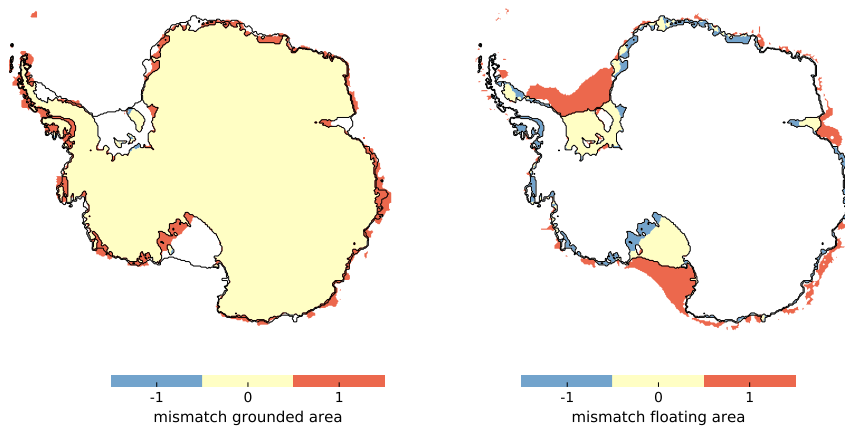
Figure 13: Comparison of present-day grounded (left) and floating (right) ice extent in best fit ensemble simulation with respect to observations (Fretwell et al., 2013). Yellow color indicate a match of simulation and observations, orange means grounded/floating in model but not in observations, and blue vise versa. Root-mean-square distance of modeled and observed grounding line is 67 km.
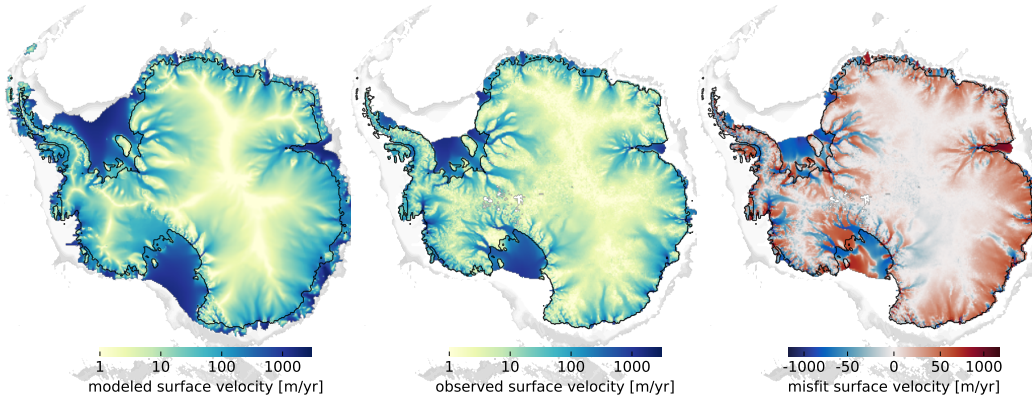
Figure 14: Comparison of present-day surface velocity in best fit ensemble simulation (left) with respect to observations (middle, Rignot et al., 2011), all in log-scale. Greenish shading indicates slow flowing regions and ice divides, blueish shading indicates regions of fast ice flow with ice shelves and far-inland reaching ice streams, respectively. Model-observations difference is shown for observed glacierized area in right panel, RMSE for surface velocities is 35 m/yr, mean misfit is 66 m/yr.

At last glacial maximum, before 10 kyr BP, the sea-level relevant volume history of the best-score simulation is close to the ensemble mean (Fig. 9). The LGM state is characterized by extended ice sheet flow towards the outer Antarctic continental shelf edges, with more than 2,000 m thicker ice than today in the basins of the largest modern ice shelves (Ross, Weddell, Amery and Amundsen), while the inner East Antarctic Ice was a few hundred meters thinner than today (see Fig. 15). At last glacial maximum around 15 kyr BP our simulations agree well with reconstructions by the RAISED Consortium (Bentley et al., 2014, cf. Fig. 7 a).

Even though this is not the primary focus of this parameter ensemble study, it is worthwhile to have a closer look into the deglacial period. The last glacial termination (also known as Termination I, which is the end of Marine isotope stage 2), and hence the period of major ice sheet retreat, initiates in our best-score simulation in the Ross and Amundsen sector at around 9 kyr BP, in the Amery sector at around 8 kyr BP and in the Weddell Sea Sector at around 7 kyr BP. Maximum change rates are found accordingly in the period 10–8 kyr BP with -1.4 mm/yr SLE (or -660 Gt/yr) in the period 8–6 kyr BP with -2.4 mm/yr SLE (or -1,300 Gt/yr, Fig. 16), with a peak of around -5 mm/yr SLE at 7.5 kyr BP (or -3,300 Gt/yr in the 100 yr running mean, compare black and khaki line in Fig. 17). This rate of change is significantly larger than in the ensemble mean, in which some retreat occurs throughout the Holocene (see Fig. 9 c). The total ice volume change during the period 10–5 kyr BP amounts to -9.7 m SLE. Most of this change can be attributed to increased discharge by around -1,000 Gt/yr and increased sub-shelf melting by around -450 Gt/yr (partly due to increased floating ice shelf area), while surface mass balance increased only by around 300 Gt/yr (Fig. 17). Recent

proxy-data reconstructions from the eastern Ross continental shelf suggested initial retreat not before 11.5 kyr BP (Bart et al., 2018), likely around 9–8 kyr BP (Spector et al., 2017), which is consistent with our model simulations. In the reconstructions by the RAISED Consortium most of the retreat in the Ross Sea Sector (almost up to present-day grounding line location) occurred between 10 kyr BP and 5 kyr BP, while major retreat in the Weddell Sea Sector likely happened before 10 kyr BP in scenario A and after 5 kyr BP in scenario B (Bentley et al., 2014, cf. Fig. 7 b,c).

A Holocene minimum ice volume is reached in our simulations around 3 kyr BP with slight re-advance and thickening in the Siple coast and Bungenstock ice rise until present-day (see Fig. 16). This regrowth signal cannot be inferred from RAISED reconstructions with snapshots only every 5 kyr (Bentley et al., 2014). The corresponding mass change is rather small with 60 Gt/yr (or 0.07 mm/yr SLE) in the last 3,000 years, see Fig. 17. During this late Holocene period, surface mass balance of around 3,700 Gt/yr is balanced by approximately -2,600 Gt/yr discharge, while sub-shelf melt plays a minor role with around -1,000 Gt/yr.
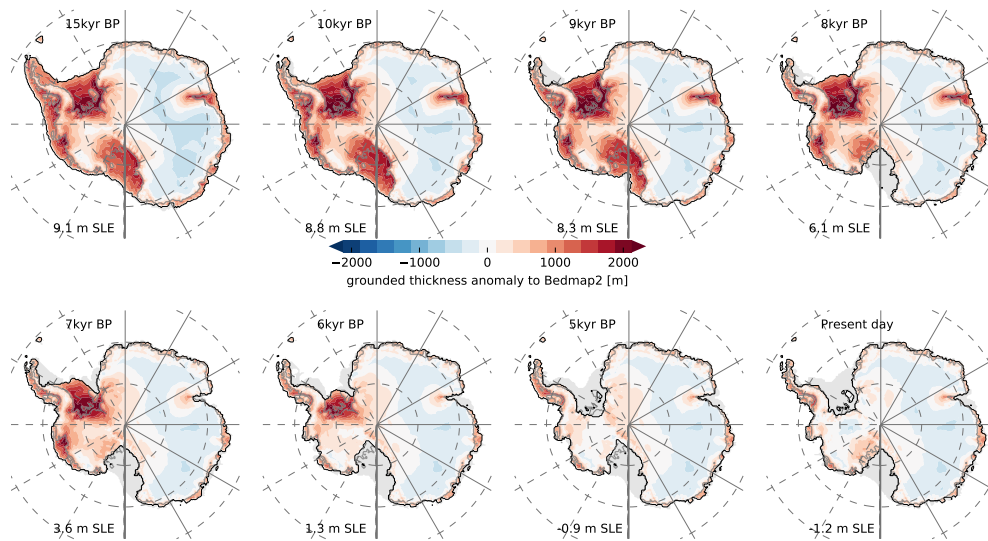
Figure 15: Snapshots of grounded ice thickness anomaly to present-day observations (Fretwell et al., 2013) over last 15 kyr in best-fit simulation, analogous to Fig. 2 in Golledge et al. (2014). At LGM state grounded ice extends towards the edge of the continental shelf with much thicker ice than present, mainly in West Antarctica. Retreat of the ice sheet occurs first in the Ross basin between 9 and 8 kyr BP, followed by the Amery basin around 1 kyr later and the Amundsen and Weddel Sea basin between 7 and 5 kyr BP. East Antarctic Ice Sheet thickness is underestimated throughout the deglaciation period (light blue shaded area).
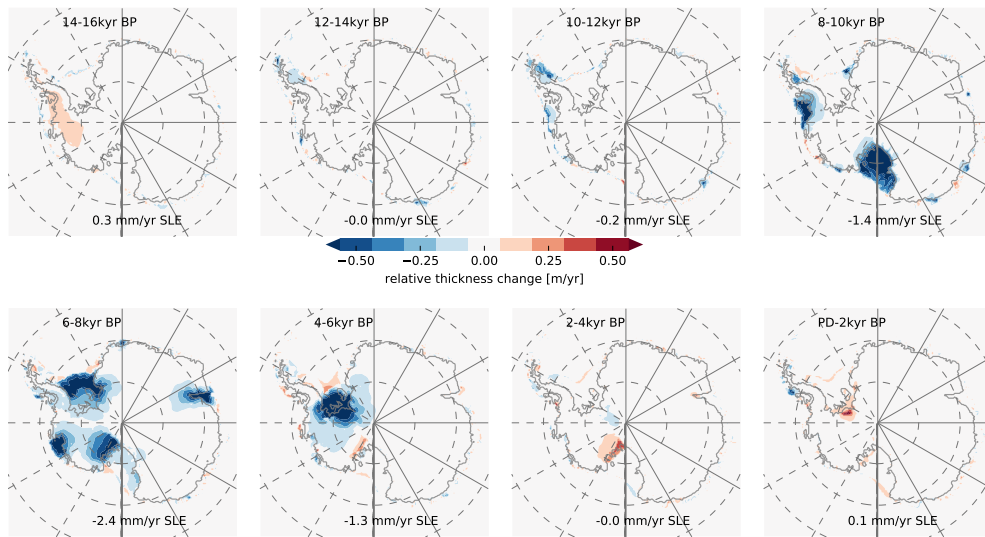
Figure 16: Snapshots of relative ice thickness change rates every 2 kyr over last 16 kyr in best-fit simulation, analogous to Fig. 4 in Golledge et al. (2014). Deglaciation starts in the Ross and Amundsen Sector after 10 kyr BP with a mean change rate of -1.4 mm/yr SLE followed by the Amery and Weddell Sea Sector after 8 kyr BP with mean change rates of up to -2.4 mm/yr SLE (with peaks of up to -5 mm/yr SLE at 7.5 kyr BP). In the late Holocene period since 4 kyr BP the best fit simulation shows some thickening in the Siple Coast and in the Bungenstock Ice Rise corresponding to about +0.1 mm/yr SLE.
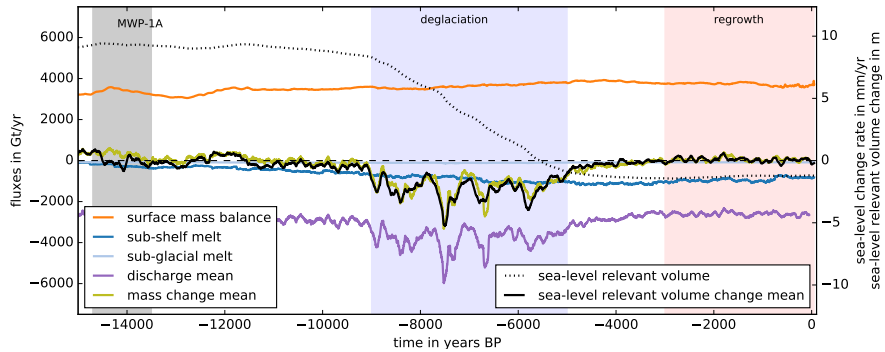
Figure 17: Mass fluxes over the last 15 kyr for the best-fit simulation (left axis), with the sum of surface (orange) and basal mass balance (blue, sub-glacial melt in light blue is negligible) and discharge (100 yr running mean in violet) yielding total mass change (khaki). Mass change agrees well with sea-level relevant volume change (100 yr running mean in black, right axis). Main deglaciation occurs between 9-5 kyr BP (black dotted line, right axis) with on average 2.0 mm/yr or 1,000 Gt/yr (blue bar), significantly after MWP-1A (grey bar). In the last 3 kyr of the best-fit simulation, the Antarctic Ice Sheet re-gains mass by about 60 Gt/yr, which equals about 0.07 mm/yr SLE (red bar).

3.4 Discussion of individual ensemble parameters

In this section we want to discuss the effects of individual ensemble parameters in more detail, also in comparison to previous model studies. We performed our analysis for an ensemble of 256 simulations of the entire Antarctic Ice Sheet over the last two glacial cycles with 16 km grid resolution using PISM. The parameter ensemble is spanned by four model parameters (Sect. 2.1), two of them are more relevant for glacial dynamics in the West Antarctic Ice Sheet (VISC and PPQ), while the other two are more related to glacial ice volume change in the East Antarctic Ice Sheet (ESIA and PREC, see overview in Sect. 2.1).

For the bedrock response we chose the upper mantle viscosity as one ensemble parameters and found maximum scores around values of $VISC = 0.5 \times 10^{21}$ Pa s for whole Antarctica. This corresponds to a rebound time scale of 1–3 thousand years, which is in line with the findings in Maris et al. (2014); Pollard et al. (2016) for WAIS, using a simplified Earth model (ELRA). Pollard et al. (2017), in contrast, used the same ensemble analysis tools for whole Antarctica, and varied the vertical viscoelastic profiles of the Earth within a gravitationally self-consistent coupled Earth-sea level model. They found only little difference in simulated glacial to modern ice volumes for different viscosity profiles bounded between 1×10^{19} Pa s and 5×10^{21} Pa s. Briggs et al. (2014) have not varied visco-elastic Earth model components, assuming that the impact of for instance climatic forcing is more relevant.

For the basal sliding we decided on the sliding exponent PPQ as uncertain ensemble parameter. A value of 0 corresponds to Coulomb friction as used in the PSU-ISM simulations, while ANICE used a value of 0.3 (Maris et al., 2014) and Quiquet et al. (2018) a linear scaling (1.0). Interestingly, we find best scores for rather high sliding exponents of PPQ with values of 0.75 or 1.0 (rather linear 525 relationship of sliding velocity and till strength).

Briggs et al. (2013) used Coulomb friction and varied instead three parameters that control the basal sliding over soft and hard beds, based on a erosion parameterization. In our study, the till weakness is associated with the till friction angle, which is optimized for the present-day grounded Antarctic Ice Sheet (Pollard and DeConto, 2012b). In Briggs et al. (2013), basal sliding additionally 530 accounts for basal roughness and pinnings points (three parameters), which is otherwise underestimated as a result of the coarse model resolution.

Another sliding-related key parameter is the friction coefficient underneath the modern ice shelves as varied in (Pollard et al., 2016, 2017), who found it to be the most dominant ensemble parameter. As discussed in the companion paper (Albrecht et al., 2019), we also find till properties in the ice 535 shelf regions highly relevant, in particular during deglaciation. As a consequence, we have run an additional ensemble analysis for four parameters associated with basal sliding and hydrology, including friction underneath modern ice shelves and discussed the results in the Supplementray Material A. In the best fit simulations of this "basal ensemble", we find main deglacial retreat occurring a few thousand years earlier (closer to MWP-1A) than in the base ensemble. Hence, the corresponding 540 scores are even better than for the best fit simulation of the base ensemble, for same sliding exponent but smaller minimal till friction angle of $\leq 1°$.

For a representation of the ice dynamical uncertainty we chose the ESIA enhancement factor as most relevant ensemble parameter, which mainly affects the grounded ice volume. We find best fits 545 for rather small ESIA of 1–2, while for larger values the modeled EAIS ice thickness underestimates modern observations. Pollard et al. (2016) did not vary enhancement factors in their ensemble and used a rather small enhancement factor of 1 for the SIA, while the value for the SSA enhancement was prescribed to a very low value of 0.3 (Pollard and DeConto, 2012a). Briggs et al. (2014) varied enhancement factors for both the SIA and SSA in their large ensemble, and determined a rather large 550 reference value of 4.8 for SIA enhancement and a reference value for SSA enhancement close to 0.6 (see Table 1 Briggs et al., 2013), which we have used in all our ensemble simulations. Maris et al. (2014) determined in their sensitivity study for the SIA enhancement an even larger reference value of 9 and for the SSA enhancement 0.8. In Quiquet et al. (2018) best fits to present-day thickness are found for SIA enhancement between 1.5 and 4, for SSA enhancement between 0.2 and 0.5 respec- 555 tively.

As climate-related uncertain ensemble parameter we chose a parameter associated with the change of precipitation with temperatures, PREC. The best-fit parameter values of PREC = 7–10 %/K yield for 10 K colder glacial temperatures about 50-65 % less precipitation. This parameter is similar to the insolation scaling parameter in Briggs et al. (2013), where the best fit value would result in about 60% less precipitation at insolation minimum. In total, Briggs et al. (2014) varied seven precipitation-related parameters based on three different precipitation forcings (one of which is similar to the one we used). Maris et al. (2014) used instead a linear temperature-based scaling between LGM and present-day surface mass balance (with about 58% anomaly) with a fixed parameter.

Beyond the four parameters varied in our ensemble, previous ensemble studies found for instance a high sensitivity in at least one of the five temperature related parameters (Briggs et al., 2013). In contrast, we found only little effect of temperature on the sea-level relevant ice sheet volume, as discussed in the companion paper (Albrecht et al., 2019). Concerning iceberg calving, Pollard et al. (2016) included one related parameter in their ensemble analysis, while Briggs et al. (2013) varied three parameters for ice shelf calving and one parameter for tidewater calving. Our 'eigencalving' parameterization also uses a strain-rate based calving estimate, combined with a minimal terminal ice thickness and provides a representation of calving front dynamics, which in first order yields calving front locations close to present observations (Levermann et al., 2012). As this parameterization is rather independent of the climate conditions, variations of the 'eigencalving' parameter show only little effect on sea-level relevant ice volume (see Albrecht et al. (2019)).

Regarding sub-shelf melting, Pollard et al. (2016) and Quiquet et al. (2018) included one uncertain parameter in their analysis, while Briggs et al. (2013) even varied four melt-related parameters. As we used the PICO model that includes physics to adequately represent melting and refreezing (Reese et al., 2018). the two key PICO parameters have been constrained for present observations, so that we have preferred other less constrained parameters in our ensemble that are more relevant for the ice volume history of the Antarctic Ice Sheet.

The four selected ensemble parameters, representing uncertainties in interacting ice-Earth dynamics, basal sliding as well climate conditions, imply a large range of uncertainty for the total Antarctic ice volume change. They have been chosen, such that the model yields a present-day ice volume close to observations, while the LGM ice volume differs significantly for parameter change. The probed parameter range has been chosen rather wide, which implies a low sampling density of the parameter space. With the knowledge gained in this ensemble analysis, this range could be further constrained in a (larger) sub-ensemble. Also, other parameters may be more relevant for certain regions of the Antarctic Ice Sheet or for the onset and rate of the last deglaciation, which in our

ensemble occurs generally later than suggested by many paleo records. A closer look into the details of the deglacial period and relevant parameters will be discussed in a separate follow-up study.

595   One deficiency of our model settings is the general underestimation of ice thickness in the inner ice sheet sections (up to -500 m, mainly in the EAIS, which could be a result of the underestimated RACMO precipitation) and an overestimation in the outer terminal regions and at Siple Coast (up to +500 m), where the complex topography is not sufficiently resolved in the model with implications for inferred basal conditions and temperature conditions. Accordingly, we find a considerable misfit

600   to most paleo elevation data (ELEV), which are located mainly in the marginal mountain regions. This could be improved, e.g. by parameterized basal roughness or erosion, as proposed in Briggs et al. (2013), or by higher model resolution and updated bed topography data sets[2].

The score aggregation scheme according to Pollard et al. (2016) implies that the paleo data types have equal influence as the present-day constraints, although they cover only relatively small regions

605   and periods of the modeled ice sheet history (Briggs and Tarasov, 2013). However, as the variability in paleo misfits is comparably low among the ensemble, these data types have only relatively small imprint on the aggregated score (see more details in Supplementary Material B). This is also valid for a data-type weighted score (Briggs and Tarasov, 2013), which applied to our ensemble results yields a similar set of best score runs.

610   Further work will consist in the determination of more realistic climate reconstruction using general circulation model results and in the explicit computation of the local relative sea-level, which could potentially have an strong impact on grounding line migration for glacial cycles (Gomez et al., 2013).

4   Conclusions

615   We have run an ensemble of 256 simulations over the last two glacial cycles and have applied a simple averaging method with full factorial sampling similar to Pollard et al. (2016). Although this kind of ensemble method is limited to a comparably small number of values for each parameter and hence the retrieved scores are somewhat blocky (as compared to advanced techniques that can interpolate in parameter space) we still recognize a general pattern of parameter combinations that

620   provide best model fits to both present-day observations and paleo records. However, the selected ensemble parameters certainly can not cover the full range of possible model response, in particular with regard to the self-amplifying effects during deglaciation.

For the four sampled parameters, best fits are found for mantle viscosity around VISC = 0.5– 2.5×10^{21} Pa s, rather linear relationships between sliding speed and till strength (with exponents

625   PPQ = 0.75–1.0), no or only small enhancement of the SIA derived flow speed (with ESIA = 1–2) and for rather high rates of relative precipitation change with temperature forcing (PREC > 5 %/K).

---

[2]https://sites.uci.edu/morlighem/bedmachine-antarctica/

The five best-score ensemble members fall within this range. In comparison to the best-fit member (VISC $= 0.5 \times 10^{21}$ Pa s, PREC $= 7$ %/K, PPQ $= 0.75$, ESIA $= 2$) slightly more sliding (PPQ $= 1$) or slower ice flow (ESIA $= 1$) can compensate for relatively dry climate conditions in colder climates for higher PREC values, which is associated with smaller ice volumes and hence smaller driving stresses. Strongest effects of varying ESIA and PREC parameters are found for the much larger East Antarctic Ice Sheet volume, while PPQ and VISC have most pronounced effects for the West Antarctic Ice Sheet dynamics in terms of grounding line migration and induced changes in ice loading.

Grounding line extends at last glacial maximum to the edge of the continental shelf for nearly all simulations. The onset and rate of deglaciation, however is very sensitive to the choice of parameters and boundary conditions, in particular those related to basal sliding. Due to the comparably coarse resolution and the high uncertainty that comes with the strong non-linearity (sensitivity) of the system, we here discuss rather general patterns of reconstructed ice sheet histories than exact numbers, which would require a much larger ensemble with an extended number of varied parameters.

The score-weighted likely range (one standard deviation) of our reconstructed ice volume histories suggest a contribution of the Antarctic Ice Sheet to the global mean sea level since the Last Glacial Maximum at around 15 kyr BP of 9.4 ± 4.1 m SLE ($6.5 \pm 2.0 \times 10^6$ km^3). The ensemble-mean ice volume anomaly between LGM and present is therewith slightly higher than in most recently published studies. The choice of basal sliding parameterization in the different models seems to have most impact on the corresponding estimates. The ensemble reproduces the observed present-day grounded ice volume with an score-weighted anomaly of 0.6 ± 3.5 m SLE ($0.7 \pm 1.7 \times 10^6$ km^3) and hence serves as a suitable inital state for future projections.

The reconstructed score-weighted ensemble range (1σ) is comparably large with up to 4.3 m SLE (or 2.0×10^6 km^3), which can be explained by a high model sensitivity (Albrecht et al., 2019), by a comparably large range of the sampled parameter values and of course due to the choice of the aggregated score scheme. By using "sieve" criteria the ensemble range can be reduced. For the much larger ensemble study by covering 31 parameters Briggs et al. (2014) a narrowed ensemble range of 4.4 mESL (different definition of sea-level equivalent volume change) or 1.8×10^6 km^3 was found for the best 5% of the ensemble simulations, which is close to the range of our study.

The onset of deglaciation and hence major grounding line retreat occurs in our model simulations after 12 kyr BP and hence well after MWP1a (≈ 14.3 kyr BP). A previous PISM study simulated much earlier and larger sea-level contributions from Antarctica for oceanic forcing at intermediate levels that is anticorrelated to the surface temperature forcing (Golledge et al., 2014), as likely happened during the two millennia of Antarctic Cold Reversal following the MWP1a.

The PISM model results in Kingslake et al. (2018) are based on this ensemble study, but have been published before with a slightly older model version (see data and model code availability therein). Meanwhile, we have improved the Earth model, which accounts for changes in the ocean water

column induced by variations in bed topography or sea-level changes. In contrast to Kingslake et al.
(2018), we used the remapped topography without local adjustment in the region of Bungenstock ice
rise in the Weddell Sea sector, and found in about 20% of the score-weighted simulations a extensive
retreat of the grounding line and subsequent re-advance in both the Ross and Weddell Sea sector.

The here presented paleo simulation ensemble analysis with PISM provides a set of data-constrained
parameter combinations, that can be used as a reference for further sensitivity studies investigating
specific episodes in the history of Antarctica, such as the the last deglaciation or the Last Interglacial,
as well as for projections of Antarctic sea-level contributions.

Author contributions

TA designed, ran and analyzed the ice sheet model experiments; TA and RW co-developed PISM and
implemented processes relevant for application to the Antarctic Ice Sheet. RW and AL contributed
to the interpretation of the results.

Code and data availability

The PISM code used in this study can be obtained from https://github.com/talbrecht/pism_pik/tree/
pism_pik_1.0 and will be published with DOI reference. Results and plotting scripts are available
upon request and will be published in www.PANGAEA.de. For now see jupyter notebook https://
nbviewer.jupyter.org/url/www.pik-potsdam.de/~albrecht/notebooks/paleo_paper_final2.ipynb. PISM
input data are preprocessed using https://github.com/pism/pism-ais with original data citations.

Competing interests

The authors declare that they have no conflicts of interest.

Acknowledgements. Development of PISM is supported by NASA grant NNX17AG65G and NSF grants PLR-
1603799 and PLR-1644277. Open-source software was used at all stages, in particular NumPy (www.numpy.
org), CDO (https://code.mpimet.mpg.de/projects/cdo/), NCO (http://nco.sourceforge.net/) and matplotlib (https:
//matplotlib.org/). The authors gratefully acknowledge the European Regional Development Fund (ERDF), the
German Federal Ministry of Education and Research and the Land Brandenburg for supporting this project
by providing resources on the high performance computer system at the Potsdam Institute for Climate Impact
Research. Computer resources for this project have been also provided by the Gauss Centre for Supercomput-
ing/Leibniz Supercomputing Centre (www.lrz.de) under Project-ID pr94ga and pn69ru. T.A. is supported by the
Deutsche Forschungsgemeinschaft (DFG) in the framework of the priority program "Antarctic Research with
comparative investigations in Arctic ice areas" by grant LE1448/6-1 and LE1448/7-1. We thank Dave Pollard
for sharing ensemble analysis scripts and for valueable discussions and Stewart Jamieson for sharing gridded
RAISED datasets. Finally, we appreciate the suggestions and comments by Lev Tarasov and an anonymous
reviewer, which led us to considerable improvements of the manuscript.

References

Albrecht, T., Winkelmann, R., and Levermann, A.: Glacial cycles simulation of the Antarctic Ice Sheet with PISM - Part 1: Boundary conditions and climatic forcing, The Cryosphere Discussions, 2019, doi:10.5194/tc-2019-71, https://www.the-cryosphere-discuss.net/tc-2019-71/, 2019.

Argus, D. F., Peltier, W., Drummond, R., and Moore, A. W.: The Antarctica component of postglacial rebound model ICE-6G_C (VM5a) based on GPS positioning, exposure age dating of ice thicknesses, and relative sea level histories, Geophysical Journal International, 198, 537–563, 2014.

Aschwanden, A. and Blatter, H.: Mathematical modeling and numerical simulation of polythermal glaciers, Journal of Geophysical Research: Earth Surface, 114, 2009.

Aschwanden, A., Bueler, E., Khroulev, C., and Blatter, H.: An enthalpy formulation for glaciers and ice sheets, Journal of Glaciology, 58, 441–457, doi:10.3189/2012JoG11J088, 2012.

Barletta, V. R., Bevis, M., Smith, B. E., Wilson, T., Brown, A., Bordoni, A., Willis, M., Khan, S. A., Rovira-Navarro, M., Dalziel, I., et al.: Observed rapid bedrock uplift in Amundsen Sea Embayment promotes ice-sheet stability, Science, 360, 1335–1339, 2018.

Bart, P. J., Mullally, D., and Golledge, N. R.: The influence of continental shelf bathymetry on Antarctic Ice Sheet response to climate forcing, Global and Planetary Change, 142, 87–95, 2016.

Bart, P. J., DeCesare, M., Rosenheim, B. E., Majewski, W., and McGlannan, A.: A centuries-long delay between a paleo-ice-shelf collapse and grounding-line retreat in the Whales Deep Basin, eastern Ross Sea, Antarctica, Scientific reports, 8, 12 392, 2018.

Bentley, M. J., Ó Cofaigh, C., Anderson, J. B., Conway, H., Davies, B., Graham, A. G. C., Hillenbrand, C.-D., Hodgson, D. A., Jamieson, S. S. R., Larter, R. D., Mackintosh, A., Smith, J. A., Verleyen, E., Ackert, R. P., Bart, P. J., Berg, S., Brunstein, D., Canals, M., Colhoun, E. A., Crosta, X., Dickens, W. A., Domack, E., Dowdeswell, J. A., Dunbar, R., Ehrmann, W., Evans, J., Favier, V., Fink, D., Fogwill, C. J., Glasser, N. F., Gohl, K., Golledge, N. R., Goodwin, I., Gore, D. B., Greenwood, S. L., Hall, B. L., Hall, K., Hedding, D. W., Hein, A. S., Hocking, E. P., Jakobsson, M., Johnson, J. S., Jomelli, V., Jones, R. S., Klages, J. P., Kristoffersen, Y., Kuhn, G., Leventer, A., Licht, K., Lilly, K., Lindow, J., Livingstone, S. J., Massé, G., McGlone, M. S., McKay, R. M., Melles, M., Miura, H., Mulvaney, R., Nel, W., Nitsche, F. O., O'Brien, P. E., Post, A. L., Roberts, S. J., Saunders, K. M., Selkirk, P. M., Simms, A. R., Spiegel, C., Stolldorf, T. D., Sugden, D. E., van der Putten, N., van Ommen, T., Verfaillie, D., Vyverman, W., Wagner, B., White, D. A., Witus, A. E., and Zwartz, D.: A community-based geological reconstruction of Antarctic Ice Sheet deglaciation since the Last Glacial Maximum, Quaternary Science Reviews, 100, 1–9, doi:10.1016/j.quascirev.2014.06.025, 2014.

Briggs, R., Pollard, D., and Tarasov, L.: A glacial systems model configured for large ensemble analysis of Antarctic deglaciation, The Cryosphere, 7, 1949–1970, 2013.

Briggs, R. D. and Tarasov, L.: How to evaluate model-derived deglaciation chronologies: a case study using Antarctica, Quaternary Science Reviews, 63, 109–127, 2013.

Briggs, R. D., Pollard, D., and Tarasov, L.: A data-constrained large ensemble analysis of Antarctic evolution since the Eemian, Quaternary Science Reviews, 103, 91–115, doi:10.1016/j.quascirev.2014.09.003, 2014.

Bueler, E. and Brown, J.: Shallow shelf approximation as a "sliding law" in a thermomechanically coupled ice sheet model, Journal of Geophysical Research, 114, doi:10.1029/2008JF001179, 2009.

Bueler, E. and van Pelt, W.: Mass-conserving subglacial hydrology in the Parallel Ice Sheet Model version 0.6, Geoscientific Model Development, 8, 1613, 2015.

Bueler, E., Lingle, C. S., and Brown, J.: Fast computation of a viscoelastic deformable Earth model for ice-sheet simulations, Annals of Glaciology, 46, 97–105, 2007.

740 Cuffey, K. M. and Marshall, S. J.: Substantial contribution to sea-level rise during the last interglacial from the Greenland ice sheet, Nature, 404, 591, 2000.

Cuffey, K. M. and Paterson, W. S. B.: The physics of glaciers, Academic Press, 2010.

Cuffey, K. M., Clow, G. D., Steig, E. J., Buizert, C., Fudge, T., Koutnik, M., Waddington, E. D., Alley, R. B., and Severinghaus, J. P.: Deglacial temperature history of West Antarctica, Proceedings of the National Academy
745 of Sciences, 113, 14 249–14 254, http://www.usap-dc.org/view/dataset/600377, 2016.

De Boer, B., Van de Wal, R., Lourens, L., Bintanja, R., and Reerink, T.: A continuous simulation of global ice volume over the past 1 million years with 3-D ice-sheet models, Climate Dynamics, 41, 1365–1384, 2013.

Fogwill, C., Turney, C., Golledge, N., Etheridge, D., Rubino, M., Thornton, D., Baker, A., Woodward, J., Winter, K., Van Ommen, T., et al.: Antarctic ice sheet discharge driven by atmosphere-ocean feedbacks at
750 the Last Glacial Termination, Scientific reports, 7, 39 979, 2017.

Fretwell, P., Pritchard, H. D., Vaughan, D. G., Bamber, J. L., Barrand, N. E., Bell, R., Bianchi, C., Bingham, R. G., Blankenship, D. D., Casassa, G., Catania, G., Callens, D., Conway, H., Cook, A. J., Corr, H. F. J., Damaske, D., Damm, V., Ferraccioli, F., Forsberg, R., Fujita, S., Gim, Y., Gogineni, P., Griggs, J. A., Hindmarsh, R. C. A., Holmlund, P., Holt, J. W., Jacobel, R. W., Jenkins, A., Jokat, W., Jordan, T., King, E. C.,
755 Kohler, J., Krabill, W., Riger-Kusk, M., Langley, K. A., Leitchenkov, G., Leuschen, C., Luyendyk, B. P., Matsuoka, K., Mouginot, J., Nitsche, F. O., Nogi, Y., Nost, O. A., Popov, S. V., Rignot, E., Rippin, D. M., Rivera, A., Roberts, J., Ross, N., Siegert, M. J., Smith, A. M., Steinhage, D., Studinger, M., Sun, B., Tinto, B. K., Welch, B. C., Wilson, D., Young, D. A., Xiangbin, C., and Zirizzotti, A.: Bedmap2: improved ice bed, surface and thickness datasets for Antarctica, The Cryosphere, 7, 375–393, doi:10.5194/tc-7-375-2013,
760 https://secure.antarctica.ac.uk/data/bedmap2/, 2013.

Frieler, K., Clark, P. U., He, F., Buizert, C., Reese, R., Ligtenberg, S. R. M., van den Broeke, M. R., Winkelmann, R., and Levermann, A.: Consistent evidence of increasing Antarctic accumulation with warming, Nature Climate Change, 5, 348–352, doi:10.1038/nclimate2574, 2015.

Golledge, N. R., Fogwill, C. J., Mackintosh, A. N., and Buckley, K. M.: Dynamics of the last glacial maximum
765 Antarctic ice-sheet and its response to ocean forcing, Proceedings of the National Academy of Sciences, 109, 16 052–16 056, 2012.

Golledge, N. R., Levy, R. H., McKay, R. M., Fogwill, C. J., White, D. A., Graham, A. G., Smith, J. A., Hillenbrand, C.-D., Licht, K. J., Denton, G. H., et al.: Glaciology and geological signature of the Last Glacial Maximum Antarctic ice sheet, Quaternary Science Reviews, 78, 225–247, 2013.

770 Golledge, N. R., Menviel, L., Carter, L., Fogwill, C. J., England, M. H., Cortese, G., and Levy, R. H.: Antarctic contribution to meltwater pulse 1A from reduced Southern Ocean overturning, Nature Communications, 5, doi:10.1038/ncomms6107, 00000, 2014.

Gomez, N., Pollard, D., and Mitrovica, J. X.: A 3-D coupled ice sheet–sea level model applied to Antarctica through the last 40 ky, Earth and Planetary Science Letters, 384, 88–99, 2013.

775   Jenkins, A., Shoosmith, D., Dutrieux, P., Jacobs, S., Kim, T. W., Lee, S. H., Ha, H. K., and Stammerjohn, S.: West Antarctic Ice Sheet retreat in the Amundsen Sea driven by decadal oceanic variability, Nature Geoscience, 11, 733–738, 2018.

Jouzel, J., Masson-Delmotte, V., Cattani, O., Dreyfus, G., Falourd, S., Hoffmann, G., Minster, B., Nouet, J., Barnola, J. M., Chappellaz, J., Fischer, H., Gallet, J. C., Johnsen, S., Leuenberger, M., Loulergue, L., Luethi,
780   D., Oerter, H., Parrenin, F., Raisbeck, G., Raynaud, D., Schilt, A., Schwander, J., Selmo, E., Souchez, R., Spahni, R., Stauffer, B., Steffensen, J. P., Stenni, B., Stocker, T. F., Tison, J. L., Werner, M., and Wolff, E. W.: Orbital and Millennial Antarctic Climate Variability over the Past 800,000 Years, Science, 317, 793– 796, doi:10.1126/science.1141038, 2007.

Kingslake, J., Scherer, R., Albrecht, T., Coenen, J., Powell, R., Reese, R., Stansell, N., Tulaczyk, S., Wearing,
785   M., and Whitehouse, P.: Extensive retreat and re-advance of the West Antarctic ice sheet during the Holocene, Nature, 558, 430, 2018.

Kopp, R. E., Simons, F. J., Mitrovica, J. X., Maloof, A. C., and Oppenheimer, M.: Probabilistic assessment of sea level during the last interglacial stage, Nature, 462, 863–867, 2009.

Levermann, A., Albrecht, T., Winkelmann, R., Martin, M., Haseloff, M., and Joughin, I.: Kinematic first-order
790   calving law implies potential for abrupt ice-shelf retreat, The Cryosphere, 6, 273–286, 2012.

Lingle, C. S. and Clark, J. A.: A numerical model of interactions between a marine ice sheet and the solid earth: Application to a West Antarctic ice stream, Journal of Geophysical Research: Oceans, 90, 1100–1114, 1985.

Liu, J., Milne, G. A., Kopp, R. E., Clark, P. U., and Shennan, I.: Sea-level constraints on the amplitude and source distribution of Meltwater Pulse 1A, Nature Geoscience, 9, 130–134, doi:10.1038/ngeo2616, 2016.

795   Maris, M., De Boer, B., Ligtenberg, S., Crucifix, M., Van De Berg, W., and Oerlemans, J.: Modelling the evolution of the Antarctic ice sheet since the last interglacial, The Cryosphere, 8, 1347–1360, 2014.

Maris, M., Van Wessem, J., Van De Berg, W., De Boer, B., and Oerlemans, J.: A model study of the effect of climate and sea-level change on the evolution of the Antarctic Ice Sheet from the Last Glacial Maximum to 2100, Climate dynamics, 45, 837–851, 2015.

800   Martos, Y. M., Catalán, M., Jordan, T. A., Golynsky, A., Golynsky, D., Eagles, G., and Vaughan, D. G.: Heat flux distribution of Antarctica unveiled, Geophysical Research Letters, 44, 2017.

Mercer, J. H.: West Antarctic ice sheet and CO2 greenhouse effect: a threat of disaster, Nature, 271, 321, 1978.

Morland, L. and Johnson, I.: Steady motion of ice sheets, Journal of Glaciology, 25, 229–246, 1980.

Oppenheimer, M. and Alley, R. B.: How high will the seas rise?, Science, 354, 1375–1377, 2016.

805   Pattyn, F.: The paradigm shift in Antarctic ice sheet modelling, Nature communications, 9, 2728, 2018.

Pollard, D. and DeConto, R.: Description of a hybrid ice sheet-shelf model, and application to Antarctica, Geoscientific Model Development, 5, 1273, 2012a.

Pollard, D. and DeConto, R. M.: A simple inverse method for the distribution of basal sliding coefficients under ice sheets, applied to Antarctica, The Cryosphere, 6, 953–971, doi:10.5194/tc-6-953-2012, http://www.
810   the-cryosphere.net/6/953/2012/, 2012b.

Pollard, D., Chang, W., Haran, M., Applegate, P., and DeConto, R.: Large ensemble modeling of the last deglacial retreat of the West Antarctic Ice Sheet: comparison of simple and advanced statistical techniques, Geosci. Model Dev., 9, 1697–1723, doi:10.5194/gmd-9-1697-2016, 2016.

Pollard, D., Gomez, N., and Deconto, R. M.: Variations of the Antarctic Ice Sheet in a Coupled Ice Sheet-Earth-Sea Level Model: Sensitivity to Viscoelastic Earth Properties, Journal of Geophysical Research: Earth Surface, 122, 2124–2138, 2017.

Quiquet, A., Punge, H. J., Ritz, C., Fettweis, X., Gallée, H., Kageyama, M., Krinner, G., Salas y Mélia, D., and Sjolte, J.: Sensitivity of a Greenland ice sheet model to atmospheric forcing fields, The Cryosphere, 6, 999–1018, doi:10.5194/tc-6-999-2012, https://www.the-cryosphere.net/6/999/2012/, 2012.

Quiquet, A., Dumas, C., Ritz, C., Peyaud, V., and Roche, D. M.: The GRISLI ice sheet model (version 2.0): calibration and validation for multi-millennial changes of the Antarctic ice sheet, Geoscientific Model Development, 11, 5003, 2018.

Reeh, N.: Parameterization of melt rate and surface temperature in the Greenland ice sheet, Polarforschung, 59, 113–128, 1991.

Reese, R., Albrecht, T., Mengel, M., Asay-Davis, X., and Winkelmann, R.: Antarctic sub-shelf melt rates via PICO, The Cryosphere, 12, 1969, 2018.

Rignot, E., Mouginot, J., and Scheuchl, B.: Ice Flow of the Antartctic Ice Sheet, Science, 333, 1423–1427, doi:10.1126/science.1208336, 2011.

Ritz, C., Fabre, A., and Letréguilly, A.: Sensitivity of a Greenland ice sheet model to ice flow and ablation parameters: consequences for the evolution through the last climatic cycle, Climate Dynamics, 13, 11–23, 1996.

Rutt, I. C., Hagdorn, M., Hulton, N., and Payne, A.: The Glimmer community ice sheet model, Journal of Geophysical Research: Earth Surface, 114, 2009.

Schmidtko, S., Heywood, K. J., Thompson, A. F., and Aoki, S.: Multidecadal warming of Antarctic waters, Science, 346, 1227–1231, 2014.

Schoof, C.: Ice sheet grounding line dynamics: Steady states, stability, and hysteresis, Journal of Geophysical Research, 112, doi:10.1029/2006JF000664, http://doi.wiley.com/10.1029/2006JF000664, 2007.

Seroussi, H., Nowicki, S., Simon, E., Abe Ouchi, A., Albrecht, T., Brondex, J., Cornford, S., Dumas, C., Gillet-Chaulet, F., Goelzer, H., Golledge, N. R., Gregory, J. M., Greve, R., Hoffman, M. J., Humbert, A., Huybrechts, P., Kleiner, T., Larour, E., Leguy, G., Lipscomb, W. H., Lowry, D., Mengel, M., Morlighem, M., Pattyn, F., Payne, A. J., Pollard, D., Price, S., Quiquet, A., Reerink, T., Reese, R., Rodehacke, C. B., Schlegel, N.-J., Shepherd, A., Sun, S., Sutter, J., Van Breedam, J., van de Wal, R. S. W., Winkelmann, R., and Zhang, T.: initMIP-Antarctica: An ice sheet model initialization experiment of ISMIP6, The Cryosphere Discussions, 2019, 1–44, doi:10.5194/tc-2018-271, https://www.the-cryosphere-discuss.net/tc-2018-271/, 2019.

Shepherd, A. and Nowicki, S.: Improvements in ice-sheet sea-level projections, Nature Climate Change, 7, 672, 2017.

Shepherd, A., Fricker, H. A., and Farrell, S. L.: Trends and connections across the Antarctic cryosphere, Nature, 558, 223, 2018a.

Shepherd, A., Ivins, E., Rignot, E., Smith, B., van den Broeke, M., Velicogna, I., Whitehouse, P., Briggs, K., Joughin, I., Krinner, G., et al.: Mass balance of the Antarctic Ice Sheet from 1992 to 2017, Nature, 556, pages219–222, 2018b.

Siegert, M. J., Kingslake, J., Ross, N., Whitehouse, P. L., Woodward, J., Jamieson, S. S., Bentley, M. J., Winter, K., Wearing, M., Hein, A. S., et al.: Major ice-sheet change in the Weddell Sector of West Antarctica over the last 5000 years, Reviews of Geophysics, 2019.

855 Simmons, A.: ERA-Interim: New ECMWF reanalysis products from 1989 onwards, ECMWF newsletter, 110, 25–36, 2006.

Slangen, A., Adloff, F., Jevrejeva, S., Leclercq, P., Marzeion, B., Wada, Y., and Winkelmann, R.: A review of recent updates of sea-level projections at global and regional scales, Surveys in Geophysics, 38, 385–406, 2017.

860 Spector, P., Stone, J., Cowdery, S. G., Hall, B., Conway, H., and Bromley, G.: Rapid early-Holocene deglaciation in the Ross Sea, Antarctica, Geophysical Research Letters, 44, 7817–7825, 2017.

Stuhne, G. and Peltier, W.: Assimilating the ICE-6G_C Reconstruction of the Latest Quaternary Ice Age Cycle Into Numerical Simulations of the Laurentide and Fennoscandian Ice Sheets, Journal of Geophysical Research: Earth Surface, 122, 2324–2347, 2017.

865 Stuhne, G. R. and Peltier, W. R.: Reconciling the ICE-6G_C reconstruction of glacial chronology with ice sheet dynamics: The cases of Greenland and Antarctica, Journal of Geophysical Research: Earth Surface, 120, 2015JF003 580, doi:10.1002/2015JF003580, 2015.

Sutter, J., Gierz, P., Grosfeld, K., Thoma, M., and Lohmann, G.: Ocean temperature thresholds for Last Interglacial West Antarctic Ice Sheet collapse, Geophysical Research Letters, 43, 2675–2682, 2016.

870 Tarasov, L. and Peltier, W. R.: Greenland glacial history, borehole constraints, and Eemian extent, Journal of Geophysical Research: Solid Earth, 108, 2003.

The PISM authors: PISM, a Parallel Ice Sheet Model: User's Manual, http://pism-docs.org/sphinx/, based on revision stable v.1.0 edn., 2017.

Weber, M. E., Clark, P. U., Kuhn, G., Timmermann, A., Sprenk, D., Gladstone, R., Zhang, X., Lohmann, G.,
875 Menviel, L., Chikamoto, M. O., Friedrich, T., and Ohlwein, C.: Millennial-scale variability in Antarctic ice-sheet discharge during the last deglaciation, Nature, 510, 134–138, doi:10.1038/nature13397, 00002, 2014.

Weertman, J.: Stability of the junction of an ice sheet and an ice shelf, Journal of Glaciology, 13, 3–11, 1974.

Wessem, J. M. v., Berg, W. J. v. d., Noël, B. P., Meijgaard, E. v., Amory, C., Birnbaum, G., Jakobs, C. L., Krüger, K., Lenaerts, J., Lhermitte, S., et al.: Modelling the climate and surface mass balance of polar ice
880 sheets using RACMO2–Part 2: Antarctica (1979–2016), The Cryosphere, 12, 1479–1498, 2018.

Whitehouse, P. L., Bentley, M. J., and Le Brocq, A. M.: A deglacial model for Antarctica: geological constraints and glaciological modelling as a basis for a new model of Antarctic glacial isostatic adjustment, Quaternary Science Reviews, 32, 1–24, 2012a.

Whitehouse, P. L., Bentley, M. J., Milne, G. A., King, M. A., and Thomas, I. D.: A new glacial isostatic ad-
885 justment model for Antarctica: calibrated and tested using observations of relative sea-level change and present-day uplift rates, Geophysical Journal International, 190, 1464–1482, 2012b.

Winkelmann, R., Martin, M. A., Haseloff, M., Albrecht, T., Bueler, E., Khroulev, C., and Levermann, A.: The Potsdam Parallel Ice Sheet Model (PISM-PIK) – Part 1: Model description, The Cryosphere, 5, 715–726, doi:10.5194/tc-5-715-2011, 2011.

890 Zwally, H., Li, J., Robbins, J., Saba, J., Yi, D., and Brenner, A.: Mass gains of the Antarctic ice sheet exceed losses, Journal of Glaciology, 61, doi:doi: 10.3189/2015JoG15J071, http://www.ingentaconnect.com/content/igsoc/jog/pre-prints/content-ings_jog_15j071, 2015.